HOKKAIDO UNIVERSITY

Title	Compartmentalization of interleukin 36 subfamily according to inducible and constitutive expression in the kidneys of a murine autoimmune nephritis model
Author(s)	Namba, Takashi; Ichii, Osamu; Nakamura, Teppei; Masum, Md Abdul; Otani, Yuki; Hosotani, Marina; Elewa, Yaser Hosny Ali; Kon, Yasuhiro
Citation	Cell and tissue research, s00441-021-03495-8 https://doi.org/10.1007/s00441-021-03495-8
Issue Date	2021-07-21
Doc URL	http://hdl.handle.net/2115/86347
Rights	This is a post-peer-review, pre-copyedit version of an article published in Cell and tissue research. The final authenticated version is available online at: http://dx.doi.org/10.1007/s00441-021-03495-8
Type	article (author version)
File Information	Cell and tissue researchs00441-021-03495-8.pdf

Instructions for use

Hokkaido University Collection of Scholarly and Academic Papers : HUSCAP

Title page

Compartmentalization of Interleukin 36 subfamily according to inducible and constitutive expression in the kidneys of a murine autoimmune nephritis model

Takashi Namba[1], Osamu Ichii[1,2]*, Teppei Nakamura[1,3], Md. Abdul Masum[1,4], Yuki Otani[1], Marina Hosotani[5], Yaser Hosny Ali Elewa[1,6], and Yasuhiro Kon[1]

1. Laboratory of Anatomy, Department of Basic Veterinary Sciences, Faculty of Veterinary Medicine, Hokkaido University, Sapporo, Hokkaido, 060-0818, Japan
2. Laboratory of Agrobiomedical Science, Faculty of Agriculture, Hokkaido University, Sapporo, Hokkaido, 060-8589, Japan
3. Section of Biological Safety Research, Chitose Laboratory, Japan Food Research Laboratories, Chitose, Hokkaido, 066-0052, Japan
4. Department of Anatomy, Histology and Physiology, Faculty of Animal Science and Veterinary Medicine, Sher-e-Bangla Agricultural University, Dhaka, 1207, Bangladesh
5. Laboratory of Veterinary Anatomy, Department of Veterinary Medicine, Rakuno Gakuen University, Ebetsu, Hokkaido, 069-8501, Japan
6. Department of Histology and Cytology, Faculty of Veterinary Medicine, Zagazig University, 44519, Egypt

***Corresponding author**: Osamu Ichii, D.V.M., Ph.D.

Laboratory of Anatomy, Department of Basic Veterinary Sciences, Faculty of Veterinary

Medicine, Hokkaido University, Kita 18-Nishi 9, Kita-ku, Sapporo, Hokkaido, 060-0818, JAPAN.

Tel & Fax: +81-11-706-5189, Email: ichi-o@vetmed.hokudai.ac.jp

Acknowledgments and Funding Information

This study was supported in part by JSPS KAKENHI (grant numbers JP20J22559 [Mr. Namba], 18H02331 and 19K22352 [Dr. Ichii]). The research described in this paper was chosen for the Encouragement Award at the 162nd Japanese Association of Veterinary Anatomists in Ibaraki (10-12th September 2019).

Abstract

The interleukin (IL) 36 subfamily belongs to the IL-1 family and is comprised of agonists (IL-36α, IL-36β, IL-36γ) and antagonists (IL-36Ra, IL-38). We previously reported IL-36α overexpression in renal tubules of chronic nephritis mice. To understand the localization status and biological relationships among each member of the IL-36 subfamily in the kidneys, MRL/MpJ-*Fas*$^{lpr/lpr}$ mice were investigated as autoimmune nephritis models using pathology-based techniques. MRL/MpJ-*Fas*$^{lpr/lpr}$ mice exhibited disease onset from 3 months and severe nephritis at 6-7 months (early and late stages, respectively). Briefly, IL-36γ and IL-36Ra were constitutively expressed in murine kidneys, while the expression of IL-36α, IL-36β, IL-36Ra, and IL-38 was induced in MRL/MpJ-*Fas*$^{lpr/lpr}$ mice. IL-36α expression was significantly increased and localized to injured tubular epithelial cells (TECs). CD44^{+}-activated parietal epithelial cells (PECs) also exhibited higher IL-36α positive rates, particularly in males. IL-36β and IL-38 are expressed in interstitial plasma cells. Quantitative indices for IL-36α and IL-38 positively correlated with nephritis severity. Similar to IL-36α, IL-36Ra localized to TECs and PECs at the late stage; however, MRL/MpJ-*Fas*$^{lpr/lpr}$ and healthy MRL/MpJ mice possessed IL-36Ra^{+}-smooth muscle cells in kidney arterial tunica media at both stages. IL-36γ was constitutively expressed in renal sympathetic axons regardless of strain and stage. IL-36 receptor gene was ubiquitously expressed in the kidneys and was induced proportional to disease severity. MRL/MpJ-*Fas*$^{lpr/lpr}$ mice kidneys

possessed significantly upregulated IL-36 downstream candidates, including NF-κB- or MAPK-pathway organizing molecules. Thus, the IL-36 subfamily contributes to homeostasis and inflammation in the kidneys, and especially, an IL-36α-dominant imbalance could strongly impact nephritis deterioration.

Keywords: Nephritis; Systemic autoimmune disease; Chronic kidney disease; Inflammatory cytokine; Interleukin 36

List of abbreviations

Actb: beta-actin

α-SMA: alpha smooth muscle actin

BUN: blood urea nitrogen

CKD: chronic kidney disease

Cr: creatinine

dsDNA: double stranded DNA)

DT: distal tubule

GO: gene ontology

HNF-4α: hepatic nuclear factor 4, alpha

IF: immunofluorescence

IHC: immunohistochemistry

IL: interleukin

ISH: *in situ* hybridization

MAPK: mitogen-activated protease

MD: macula densa

MRL/lpr: MRL/MpJ-$Fas^{lpr/lpr}$

MRL/+: MRL/MpJ

NF-κB: nuclear factor kappa B

PAS-H: periodic acid Schiff-hematoxylin

PBS: phosphate-buffered saline

PEC: parietal epithelial cell

PT: proximal tubule

qPCR: quantitative polymerase chain reaction

R: receptor

Ra: receptor antagonist

RC: renal corpuscle

SE: standard error

SLE: systemic lupus erythematosus

S/B ratio: weight ratio of spleen to body

TEC: tubular epithelial cell

TIL: tubulointerstitial lesion

uACR: urinary albumin to creatinine ratio

UUO: unilateral ureteral obstruction

1. Introduction

Chronic kidney disease (CKD) is caused by various factors, such as hypertension, drug use, and certain infections (Webster et al. 2017; Chen et al. 2019). Immunological alternations are closely associated with CKD development. For example, a complication of nephritis is frequently observed in systemic lupus erythematosus (SLE), a chronic autoimmune disease characterized by damaged systemic organs including the skin, spleen, kidneys, and/or central nervous system in conjunction with autoantibody production (Yu et al. 2014). It has been reported that nephritis develops in approximately 50% of SLE patients (Almaani et al. 2017). Renal histopathological changes in CKD manifest as glomerular and/or tubulointerstitial lesions (TILs), and their features differ among the various types of renal diseases. Further, CKD development is strongly mediated by inflammatory cytokines and chemokines such as interleukin (IL) 1, tumor necrosis factor α, and interferon γ, and these factors are primarily produced by kidney resident cells and hematopoietic cells recruited during inflammation (Ramesh and Reeves 2004; Iwata et al. 2011).

The IL-1 family plays crucial roles in acute and chronic inflammation. In humans, this family is composed of 7 agonists (IL-1α, IL-1β, IL-18, IL-33, IL-36α, IL-36β, and IL-36γ) and 4 antagonists (IL-1 receptor antagonist [Ra], IL-36Ra, IL-37, and IL-38), while mice lack IL-37 function (Garlanda et al. 2013). Although these cytokines are produced in response to inflammation, some of the IL-1 family members are constitutively expressed in the mesenchymal

cells and epithelial cells of several organs (Garlanda et al. 2013; Mantovani et al. 2019). Briefly, IL-1α and IL-33 localize to type 2 alveolar epithelial cells and intestinal epithelial cells, respectively (Mantovani et al. 2019). The IL-1 family is regulated through protein processing and by maintaining a balance between IL-1 family agonists and antagonists. Thus, an imbalance in IL1 family members is induced during pathological development due to inflammation and genetic mutation, ultimately leading to disease progression (Mantovani et al. 2019).

Our previous study revealed that IL-36α was overexpressed in injured epithelial cells of the distal tubules (DTs) in several murine models of nephritis including MRL/lpr mice (Ichii et al. 2010, 2017). The IL-36 subfamily of the IL-1 family is comprised of IL-36α, IL-36β, IL-36γ, and IL-36Ra, which are also known as IL-1F6, IL-1F8, IL-1F9, and IL-1F5, respectively. All of the members of the IL-36 subfamily can bind to the IL-36 receptor (IL-36R) (Garlanda et al. 2013). IL-36α, IL-36β, and IL-36γ function as agonists for IL-36R, and IL-36Ra in turn functions as their antagonist. Additionally, IL-38 (known as IL-1F10) is the putative antagonist for IL-36R, as it can bind to IL-36R and inhibit IL-36 signaling (Garlanda et al. 2013; Queen et al. 2019). It has been reported that IL-36 agonists promote inflammatory responses in the lungs, skin, kidneys, and joints by activating mitogen-activated protease (MAPK) and nuclear factor kappa B (NF-κB), and all IL-36 cytokines in the skin and IL-36γ in the intestine are constitutively expressed to facilitate the host response to infection (Ahsan et al. 2018; Queen et al. 2019). In the kidneys,

IL-36α expression positively correlates with the progression of TILs, including cell death, cell infiltration, and fibrosis in murine kidneys with unilateral ureteral obstruction (UUO). *In vitro* experiments have shown that IL-36α production is induced in epithelial cells of DT by lipopolysaccharide, a toll-like receptor ligand (Ichii et al. 2017). Another study revealed that TILs were ameliorated in an IL-36R knockout mouse model with UUO or with renal ischemia-reperfusion injury (Chi et al. 2017; Nishikawa et al. 2018). Furthermore, IL-36α levels were also increased in the kidneys and urine of patients with both acute kidney injury and CKD (Chi et al. 2017; Nishikawa et al. 2018). In regard to IL-38 function in the kidney, the injection improved the glomerular damage in MRL/MpJ-*Fas*$^{lpr/lpr}$ (MRL/lpr) mice, which are representative autoimmune disease-prone mice that are characterized by severe lymphadenopathy, splenomegaly, and glomerular nephritis; however, it must be noted that the presence of IL-38-producing cells remains undetermined in the kidney (Cohen and Eisenberg 1991; Chu et al. 2017). These studies suggest that the IL-36 subfamily is involved in the development of renal disorders and has potential for use as a novel target for the treatment and diagnosis of various renal diseases.

In other tissues, the molecular crosstalk between IL-36 cytokines and disease development has been more thoroughly characterized. Psoriasis is an immune-mediated inflammatory skin condition that exhibits an upregulation of IL-36α, IL-36β, IL-36γ, and IL-36Ra primarily in the

keratinocytes of human patients and mouse models (Blumberg et al. 2007, 2010; Johnston et al. 2011). Furthermore, IL-36Ra knockout mice presented with a more severe phenotype of psoriatic skin (Blumberg et al. 2007). In patients with SLE, the serum levels of IL-36α and IL-36γ were positively correlated with the SLE disease activity index, although that of IL-36Ra was decreased (Chu et al. 2015; Mai et al. 2018). Therefore, the expression patterns of the IL-36 subfamily appear to differ among disease types. Additionally, it has been reported that IL-1 family members can induce production of other family members, as IL-1α can stimulate IL-36α to induce inflammation in the skin (Garlanda et al. 2013; Milora et al. 2015). Although it is possible that IL-36 subfamily members closely interact with each other in the kidneys, their fine localization and biological functions remain unclear.

Here, we investigated MRL/lpr and MRL/MpJ (MRL/+) as a murine model of autoimmune nephritis and a healthy control, respectively. This study revealed differences in the localization of IL-36 subfamily cytokines. Specifically, IL-36γ and IL-36Ra were constitutively expressed in murine kidneys, while IL-36α, IL-36β, IL-36Ra, and IL-38 were induced in MRL/lpr mice. These finding suggest that the IL-36 subfamily is associated with both homeostasis and inflammation in the kidneys.

2. Material and methods

2.1. Animals and sample collection

Male and female MRL/+ and MRL/lpr mice at 3-7 months were purchased from Japan SLC, Inc. (Hamamatsu, Japan) and were maintained under specific pathogen-free conditions. All animal experimentation was approved by the Institutional Animal Care and Use Committee of the Graduate School of Veterinary Medicine, Hokkaido University (approval No.16-0124, 20-0012). Experimental animals were handled in accordance with the Guide for the Care and Use of Laboratory Animals, Graduate School of Veterinary Medicine, Hokkaido University (approved by the Association for Assessment and Accreditation of Laboratory Animal Care International). Urine was collected by pressure urination and stored at -30°C. Under deep anesthesia using a mixture of medetomidine (0.3 mg/kg), midazolam (4 mg/kg), and butorphanol (5 mg/kg), body weight was measured, and blood samples were collected from the femoral arteries. The mice were then euthanized by cervical dislocation. The weights of the spleens were measured, and then the weight ratio of spleen to body (S/B ratio) was calculated.

2.2. Serological analysis and urinalysis

Serum levels of anti-double stranded DNA (dsDNA) antibody were measured as an index of systemic autoimmune condition using an LBIS Anti-dsDNA-Mouse ELISA Kit (FUJIFILM

Wako Pure Chemical Corporation, Osaka, Japan) according to the manufacturer's instructions. Serum concentrations of creatinine (Cr) and blood urea nitrogen (BUN) were determined using a Fuji Dri-Chem 7000v instrument (FUJIFILM Medical Co., Ltd., Osaka, Japan) according to the manufacturer's instructions. Urinary levels of Cr and albumin were measured using a Urinary Creatinine Assay Kit (Detroit R&D, Inc., Detroit, MI, USA) and an LBIS Mouse Albumin ELISA Kit (FUJIFILM Wako Pure Chemical Corporation), respectively, and the urinary albumin-to-creatinine ratio (uACR) was then calculated.

2.3. Histological analysis

Kidneys were fixed overnight using 10% neutral buffered formalin at room temperature or 4% paraformaldehyde at 4°C. Specimens were routinely dehydrated using ethanol and then embedded in paraffin. Paraffin sections (2-μm thick) fixed with 10% neutral buffered formalin were prepared and stained with periodic acid Schiff-hematoxylin (PAS-H) to analyze renal histopathology.

2.4. Immunohistochemistry (IHC) and immunofluorescence (IF)

IHC and/or IF analyses for B220, CD3, Iba-1, Gr-1, CD138, CD44, alpha smooth muscle actin (α-SMA), tyrosine hydroxylase, calbindin-D28k, hepatic nuclear factor 4 alpha (HNF-4α),

200 and phosphorylated (p)-NF-κB-p65 were performed to detect B-cells, T-cells, macrophages,
201 neutrophils, plasma cells, activated parietal epithelial cells (PECs), smooth muscle cells,
202 sympathetic neurons, distal convoluted tubules, proximal tubules (PTs), and activated NF-κB-p65,
203 respectively. Similar assays for IL-36α, IL-36β, IL-36γ, IL-36Ra, and IL-38 were also performed
204 for the localization analysis. Paraffin sections (2-μm thick) fixed with 4% paraformaldehyde were
205 deparaffinized and then antigen retrieved. To block internal peroxidase activity for IHC, the
206 sections were soaked in methanol containing 0.3% H_2O_2 for 20 min at room temperature. After
207 washing three times in phosphate-buffered saline (PBS), the sections were incubated with
208 blocking serum for 1 h at room temperature to block the non-specific sites. Then, sections were
209 incubated with primary antibodies overnight at 4°C. Subsequently, the sections were washed
210 three times in PBS and were then incubated with secondary antibodies for 30 min at room
211 temperature. After washing three times in PBS, the sections for IHC were incubated with
212 streptavidin-conjugated horseradish peroxidase (SABPO(R) kit; Nichirei, Tokyo, Japan) for 30
213 min at room temperature and subsequently washed three times in PBS. Then, the immunopositive
214 reaction was visualized using 3,3'-diaminobenzidine tetrahydrochloride-H_2O_2 solution. Finally,
215 the sections were lightly stained with hematoxylin. For IF, the tissue sections were incubated with
216 Hoechst 33342 (1:500; FUJIFILM Wako Pure Chemical Corporation) for nuclear staining at
217 room temperature for 30 min and then washed three times. This was followed by examinations

under an All-in-one Fluorescence Microscope BZ-X710 (Keyence, Osaka, Japan). The details of the antibodies, antigen retrieval, blocking and combination of multiple IFs are listed in Supplemental Table 1, and Supplemental Figure 1 shows the immunostaining results of the IL-36 subfamily compared to the staining of each control immunoglobulin G.

2.5. In situ hybridization (ISH)

For ISH, formalin-fixed paraffin-embedded sections were assessed using an RNAscope 2.5 assay following the manufacturer's instructions, and all reagents and equipment for hybridization was purchased from Advanced Cell Diagnostics, Inc. (Hayward, CA, USA). Paraffin sections (5-μm thick) fixed with 10% neutral buffered formalin were air-dried overnight and then baked in HybEZ II oven for 1 h at 60°C. All procedures for ISH were performed using RNAscope 2.5 HD Reagent Kit-BROWN following the manufacturer's instructions. RNAscope Target probe-Mm-Ilrl2 (Mouse, Cat. No. 403761), RNAscope positive control probe-Mm-Polr2a (Cat. No. 312471), and RNAscope negative control probe-DapB (Cat. No. 310043) was used. Further, we performed ISH for *Il1rl2* followed by PAS-H staining to distinguish between PTs and DTs.

2.6. Histoplanimetry

In PAS-H stained sections, 30 glomeruli that showed a vascular and/or urinary pole were

selected, and the number of nuclei in the glomerulus, the size, and the area ratio of PAS^+ mesangium to glomerulus were all measured and calculated using NDP. view2 (Hamamatsu Photonics Co., Ltd., Hamamatsu, Japan) and a BZ-X Analyzer (Keyence). To evaluate infiltrated cells, including $B220^+$ B-cells, $CD3^+$ T-cells, $Iba\text{-}1^+$ macrophages, and $Gr\text{-}1^+$ neutrophils, the number was counted within 30 glomeruli with a vascular and/or urinary pole using NDP.view2. These cells were also counted in 20 tubulointerstitial areas at 400× magnification, which were first selected in the renal cortex at 4× magnification and then replaced to exclude glomeruli, and the averages per area were then calculated. For quantification of IL-36α, the number of IL-36α^+ tubules and renal corpuscles (RCs) in the cortex area was calculated in 3 sections from each mouse. Then, the number of IL-36α^+ tubules was divided by the cortex area, and the ratio of IL-36α^+ RCs number to total RCs number was calculated. In 25 RCs from each male MRL/lpr at 6-7 months, the IL-36α^+ PEC ratio was examined in CD44 positive or negative PECs using a BZ-X Analyzer. To evaluate IL-38, the number of positive cells was counted in 20 tubulointerstitial areas at 400x magnification using NDP. view2, and the averages per area were then calculated.

2.7. Quantitative polymerase chain reaction (qPCR)

Kidneys were soaked in RNA later solution (Thermo Fisher Scientific, Waltham, MA, USA)

254 at 4°C and then stored at -80°C after the solution was removed. Total RNA from kidneys was
255 purified using TRIzol reagent (Thermo Fisher Scientific) following the manufacturer's
256 instructions. The purified total RNA was treated as a template to synthesize cDNA using
257 ReverTra Ace qPCR RT Master Mix (Toyobo Co., Ltd., Osaka, Japan). qPCR analysis was
258 performed on the cDNA (20 ng/μl) using THUNDERBIRD® SYBR® qPCR Mix (Toyobo Co.,
259 Ltd.) and gene-specific primers (Supplemental Table 2). The qPCR cycling conditions were as
260 follows: 95°C for 1 min, (95°C for 15 s, 60°C for 45 s [40 cycles]). The data were normalized
261 according to the values of beta-actin (*Actb*), and those of female MRL/+ mice at 3 months using
262 the delta-delta Ct method.
263
264 ***2.8. Microarray analysis***
265 Similar to the qPCR analysis, total RNA was isolated from the kidneys of female MRL/+ and
266 MRL/lpr mice at 6 months (n= 3). RNA integrity was validated using an Agilent 2100
267 Bioanalyzer II (Agilent Technologies, Santa Clara, CA, USA), and complementary RNA was
268 synthesized using a Low Input Quick Amp Labeling Kit (Agilent Technologies). Gene expression
269 was analyzed using an Agilent Technologies Microarray Scanner and SurePrint G3 Mouse 8x60K
270 v2.0 (Agilent Technologies), and the raw data were normalized through the use of a 75Percentile
271 shift (GeneSpring; Agilent Technologies). Toppgene Suite (https://toppgene.cchmc.org/) and

Morpheus (https://software.broadinstitute.org/morpheus/) were used for gene ontology (GO) analysis and heatmap preparation, respectively.

2.9. Statistical analysis

The results were expressed as the mean ± standard error (SE) and statistically analyzed in a non-parametric manner. The significance between 2 groups was analyzed using the Mann-Whitney *U*-test ($P < 0.05$). As an exception, the values in the microarray analysis were compared using the Student's t-test ($P < 0.05$). The correlation between 2 parameters was analyzed using Spearman’s correlation test ($P < 0.05$).

3. Results

3.1. Development of autoimmune nephritis in MRL/lpr mice

First, autoimmune disease and nephritis in MRL/lpr mice at 3 and 6-7 months were evaluated using serological, urinary, and histopathological analyses (Table1, and Supplemental Figure 2–4). In regard to indices of autoimmune disease, male and female MRL/lpr mice, regardless of age, showed significantly higher values in the S/B ratio (over 2.6-fold, $P < 0.05$ at the early stage; 7.0-fold, $P < 0.01$ at the late stage) and the serum level of anti-dsDNA antibody (over 53.5-fold, $P < 0.05$ at the early stage; 55.2-fold, $P < 0.01$ at the late stage) compared to the values observed for each sex of MRL/+ mice that served as healthy controls. Furthermore, in MRL/lpr mice, the S/B ratio in both sexes (over 2.6-fold, $P < 0.05$) and the serum level of anti-dsDNA antibody in males (over 3.1-fold, $P < 0.05$) was significantly increased with age. For renal function indices at 6-7 months, only BUN levels were significantly higher in both sexes of MRL/lpr mice compared to those values in MRL/+ mice (over 1.7-fold, $P < 0.05$). Meanwhile, there was a significant difference in renal histopathology between MRL/+ and MRL/lpr mice. At 6-7 months, both sexes of the MRL/lpr mice exhibited significantly higher values of nuclei in a glomerulus (over 1.7-fold, $P < 0.01$), glomerular size (over 1.7-fold, $P < 0.01$), the area ratio of mesangium to glomerulus (over 1.3-fold, $P < 0.05$), and the number of infiltrated cells such as $B220^+$ B-cells (over 11.3-fold, $P < 0.01$ in glomeruli; over 3.2-fold, $P < 0.05$ in

300 tubulointerstitium), $CD3^+$ T-cells (over 9.3-fold, $P < 0.01$ in glomeruli; over 4.9-fold, $P < 0.01$ in
301 tubulointerstitium), Iba-1^+ macrophages (over 9.7-fold, $P < 0.05$ in glomeruli; over 1.8-fold, $P <$
302 0.01 in tubulointerstitium), and Gr-1^+ neutrophils (over 2.9-fold, $P < 0.05$ in glomeruli; over
303 1.4-fold, $P < 0.05$ in tubulointerstitium) in glomeruli and tubulointerstitium compared to those in
304 MRL/+ mice. In MRL/lpr mice, the majority of the histopathological indices, with the exception
305 of the mesangial area ratio in the male, were significantly increased with age. Based on these
306 findings, we confirmed the development of autoimmune disease followed by nephritis in
307 MRL/lpr mice and classified both strains of mice at 3 and 6-7 months as early and late stage of
308 autoimmune nephritis, respectively.
309
310 ***3.2. Enhanced mRNA expression of Il1f6 among the IL-36 subfamily members in MRL/lpr***
311 ***kidneys***
312 The mRNA expression of the IL-36 subfamily in the kidneys was evaluated using qPCR.
313 Among the IL-1 family members expressed in the late stage of autoimmune nephritis, *Il1f6*
314 coding IL-36α was the most upregulated in both sexes of MRL/lpr mice, and the mRNA levels of
315 *Il1f6* (over 7.5-fold, $P < 0.01$), *Il1b* (over 2.1-fold, $P < 0.01$), and *Il1rn* (8.2-fold, $P < 0.01$) in
316 MRL/lpr mice were significantly higher than those observed in MRL/+ mice (Figure 1a and
317 Supplemental Figure 5). However, other IL-36 subfamily members did not show any common

318 alterations between males and females in MRL/lpr mice among strains, sexes, or in regard to
319 disease development (Figure 1b to e). For *Il1f8* coding of IL-36β, female MRL/+ mice exhibited
320 significantly decreased expression with age (under 0.8-fold, $P < 0.05$; Figure 1b). For *Il1f9* of
321 coding IL-36γ, female MRL/lpr mice at the late stage exhibited significantly higher expression
322 levels compared to those of the female and male mice at the early and late stages, respectively
323 (over 2.5-fold, $P < 0.05$; Figure 1c). For *Il1f5* coding of IL-36Ra, female MRL/+ mice and male
324 MRL/lpr mice exhibited decreased expression with aging (under 0.3-fold, $P < 0.05$), and there
325 were sex differences in MRL/+ and MRL/lpr mice at the early and late stages, respectively, and
326 these differences were more pronounced in female mice than in male mice (over 2.2-fold, $P <$
327 0.05; Figure 1d). For *Il1f10* coding of IL-38, there was no significant difference among strains,
328 stages, or disease stages (Figure 1e). Thus, as described in our previous reports, *Il1f6* in both
329 sexes of MRL/lpr mouse kidneys was the most remarkably upregulated and was most associated
330 with the progression of autoimmune nephritis among the IL-36 subfamily members (Ichii et al.
331 2010, 2017).
332
333 ***3.3. IL-36α overexpression in renal tubules of MRL/lpr mice***
334 Using immunostaining, the localization of the IL-36 subfamily in kidneys was examined.
335 Initially, IL-36α^+ reactions appeared in renal tubules from the early stage of autoimmune nephritis,

and these tubules tended to be increased in number in MRL/lpr mice as disease development progressed (Figure 2a-b'''). IL-36α$^+$ reactions localized to the cytoplasm and nucleus of renal tubular epithelial cells (TECs) and appeared first in the segment close to macula densa (MD), and IL-36α$^+$ tubules frequently exhibited dilated tubular lumens and urinary casts at the late stage, as reported in our previous studies (Figure 2c and c') (Ichii et al. 2010, 2017). As shown in Figure 2d, the number of IL-36α$^+$ tubules was significantly increased in all groups as disease progression occurred, and those in both sexes at the late stage were significantly higher in MRL/lpr mice compared to these values in MRL/+ mice (over 9.3-fold, $P < 0.05$). According to double IF staining for IL-36α and calbindin-D28k (a DT marker), IL-36α primarily localized to DT epithelial cells; however, several IL-36α$^+$ TECs did not show calbindin-D28k$^+$ reactions in IL-36α$^+$ tubules (Figure 2e-e''). Furthermore, IL-36α$^+$ TECs were also observed in HNF-4α$^+$ PT; however, this number was quite low (Figure 2f-f'').

3.4. CD44$^+$ activated PECs expressing IL-36α in male MRL/lpr mice

IL-36α also localized to PECs in Bowman's capsules, and these were more frequently observed in male MRL/lpr mice at the late stage (Figure 2b''', 3a and a'). In female mice, only MRL/lpr mice at the late stage also possessed a small number of IL-36α$^+$ PECs that exhibited cuboidal shapes. For histoplanimetry, both male strains exhibited a significantly higher ratio of

IL-36α$^+$ RCs to total RCs compared to that of the female strains at the late stage, and this ratio was the highest in male MRL/lpr mice (Figure 3b). Additionally, as shown in Supplemental Figure 6a, another autoimmune nephritis model (BXSB/MpJ-*Yaa*) also possessed IL-36α$^+$ PECs.

Next, we performed double IF for IL-36α and CD44, a marker for activated PECs that is indicative of their proliferation, migration, and matrix production (Smeets et al. 2009). CD44 was observed on the cell membranes of PECs and infiltrated cells in RCs, and IL-36α and CD44 were frequently co-localized in PECs (Figure 3c-c"). We then counted and calculated the ratio of IL-36α$^+$ PECs in CD44 positive or - negative PECs in male MRL/lpr mouse cells at the late stage. As shown in Figure 3d, IL-36α was significantly and highly co-localized with CD44 in PECs (84.17 ± 2.59%).

3.5. Localization of IL-36β and IL-36γ in plasma cells and sympathetic nerves, respectively

Next, the localization of other IL-36 agonists (IL-36β and IL-36γ) was analyzed in the kidneys. IL-36β localized to the cytoplasm of CD138$^+$ plasma cells in both sexes of MRL/lpr mice at the late stage but not at the early stage (Figure 4a-b"). However, the number of positive cells was low in the kidneys, with one or two positive cells observed in each kidney section.

IL-36γ$^+$ reactions appeared at the peri-vessels and peri-glomeruli of all groups (Figure 4c). According to double IF assays, IL-36γ was co-localized with tyrosine hydroxylase, a marker for

372 peripheral sympathetic neurons (Figure 4d-d"). We also confirmed that the IL-36γ^{+} reaction could
373 be observed in the myenteric nerve plexus of the jejunum (Supplemental Figure 6b). Interestingly,
374 there were IL-36γ positive and negative axons in the kidneys of all groups; however, we could not
375 identify constant localization patterns of IL-36γ among sexes, strains, or disease stages (Figure
376 4d-d").
377
378 ***3.6. Localization of IL-36Ra in smooth muscle cells, DT epithelial cells, and PECs***
379 We also examined the localization of IL-36 subfamily antagonists in the kidneys. For
380 IL-36Ra, all groups exhibited positive reactions in the intrarenal arteries and arterioles, and
381 IL-36Ra was localized in the cytoplasm of α-SMA^{+} smooth muscle cells within the tunica media
382 (Figure 5a-b"). However, in vasculitis lesions in MRL/lpr mice, the IL-36Ra^{+} reaction was
383 defective in a subset of these lesions with transmural cell infiltration (Figure 5c). Furthermore,
384 smooth muscle cells of arteries and bronchioles in the lungs also expressed IL-36Ra
385 (Supplemental Figure 6c). Both sexes of MRL/lpr mice at the late stage possessed IL-36Ra^{+} PECs
386 that exhibited both flat and cuboidal shapes (Figure 5d and Supplemental Figure 1d'). However,
387 we could not determine obvious sex differences in IHC, unlike the IL-36α expression in PECs. In
388 both strains at the late stage, granular IL-36Ra^{+} reactions were observed in the apical portion of
389 TECs (Figure 5e). Although female MRL/+ and male MRL/lpr mice exhibited age-related

390 decreases in *Il1f5* expression (Figure 1d), a similar tendency was not observed in regard to protein
391 expression. According to IF or IHC using serial sections, IL-36Ra co-localized with
392 calbindin-D28k but not with HNF-4α, thus indicating its expression in DTs (Figure 5f-g').
393 Furthermore, several TECs co-expressed IL-36Ra and IL-36α (Figure 5h and h').
394
395 ***3.7. IL-38 overexpression in the plasma cells of MRL/lpr mice***
396 Another IL-36R antagonist, IL-38, localized to the cytoplasm of renal interstitial cells in all
397 groups, and the expression appeared to be abundant in both sexes of MRL/lpr mice at the late
398 stage compared to that of the other groups (Figure 6a-b'''). Using serial sections followed by IHC,
399 $CD138^+$ plasma cells were positive for $IL\text{-}38^+$ reactions (Figure 6c and c'). In disagreement with
400 the mRNA analysis, both sexes of MRL/lpr mice showed that the number of $IL\text{-}38^+$ cells
401 significantly increased with the progression of nephritis (over 4.7-fold, $P < 0.05$), and at the late
402 stage, the number of $IL\text{-}38^+$ cells of MRL/lpr mice tended to be higher than that of MRL/+ mice
403 (Figure 6d). These $IL\text{-}38^+$ cells did not directly contact the $IL\text{-}36\alpha^+$ tubules (Figure 6e and e').
404
405 ***3.8. Overexpression of IL-36α and IL-38 is positively correlated with autoimmune nephritis***
406 The protein expression of IL-36α and IL-38 at the late stage of autoimmune nephritis was
407 enhanced in MRL/lpr mice compared to that in MRL/+ mice among the IL-36 subfamily

members (Figure 2, 3, and 6). Thus, we analyzed correlations between the parameters of IL-36α and IL-38 and indices for autoimmune disease, renal function, and histopathology in both sexes of MRL/lpr mice (Table 2). In regard to the number of IL-36α$^+$ tubules, there were significant positive correlations with serum levels of anti-dsDNA, uACR, the number of all infiltrated cells, particularly CD3$^+$ T-cells and Iba-1$^+$ macrophages, into the tubulointerstitium. Furthermore, IL-36α$^+$ tubules were significantly and positively correlated with BUN in females and with S/B ratio in males. In regard to the IL-36α$^+$ RC ratio, male MRL/lpr mice exhibited significant and positive correlations with all indices for autoimmune disease and glomerular injury and with uACR. In contrast, the IL-36α$^+$ RC ratio of female MRL/lpr mice was significantly and positively correlated with BUN, uACR, glomerular size, glomerular nucleus number, and mesangial area ratio. Characteristically, both sexes of MRL/lpr mice showed a significantly positive correlation between the IL-36α$^+$ RC ratio and Gr-1$^+$ neutrophil number among infiltrated cells in the glomerulus. Additionally, there was a significantly positive correlation between the number of IL-36α$^+$ tubules and the RC ratio in both sexes.

In regard to the IL-38$^+$ cell number, both sexes of MRL/lpr mice exhibited significantly positive correlations with the values of anti-dsDNA antibody, uACR, CD3$^+$ T-cells in tubulointerstitium, and IL-36α$^+$ tubules. In female MRL/lpr mice, there were also significant positive correlations between IL-38$^+$ cells and the indices for BUN, Cr, and other infiltration cells

426 into the tubulointerstitium.

427

428 ***3.9. Ubiquitous mRNA expression of Il1rl2 in murine kidneys***

429 According to our previous study, IL-36R was localized in podocytes, PTs, and DTs in healthy
430 kidneys, whereas it was observed in interstitial cells and platelets in unilateral ureteral obstruction
431 kidneys (Ichii et al. 2017). To identify the localization and induction of the IL-36R mRNA *Il1rl2*,
432 we performed ISH assays in MRL/+ and MRL/lpr mice at the late stage. *Il1rl2* localized to TECs,
433 mesangial cells, podocytes, PECs, interstitial cells, transitional epithelial cells, smooth muscle
434 cells, and endothelial cells in the kidneys of both strains from the cortex to the medulla (Figure
435 7a-b'''). In the kidneys of both sexes of MRL/lpr mice, *Il1rl2* was induced in TECs, PECs, and
436 infiltrated immune cells in glomerular and tubulointerstitial lesions and in vasculitis, and positive
437 signals in PECs tended to be higher in male MRL/lpr mice than in female mice, similar to the
438 localization pattern of IL-36α (Figure 7a-b'''). As shown in Figure 7c and c', *Il1rl2*$^{+}$ signals were
439 primarily localized in DT epithelial cells, and MRL/lpr exhibited localization in the cells in close
440 proximity to the vascular pole, including the juxtaglomerular complex. However, qPCR analysis
441 revealed that there was no difference in mRNA levels of *Il1rl2* among the groups (Figure 7d).

442

443 ***3.10. Upregulation of IL-1 family signaling in MRL/lpr kidneys***

Stimulation of IL-36R induces IL-1 family signaling, including MAPK and NF-κB (Towne et al. 2004). To detect the significant GO associated with these signaling pathways, gene expression in the kidneys at the late stage was comprehensively compared between female MRL/+ and MRL/lpr mice by microarray focusing on 2-fold upregulated genes in the latter (Figure 7e and f). As shown in Figure 7e, 25 genes associated with positive regulation of MAPK activity (GO: 0043406) were significantly upregulated in MRL/lpr mice. Furthermore, in the genes related to positive regulation of NF-κB transcription factor activity (GO: 0051092), MRL/lpr mice possessed 11 genes that were significantly upregulated compared to levels in MRL/+ mice (Figure 7f). To confirm the activation of the NF-κB pathway, we performed IHC for p-NF-κB-p65, the effective component of NF-κB (Supplemental Figure 7). Positive reactions appeared in the nuclei of TECs, PECs, and especially infiltrated cells in all groups at the late stage, and the number was abundant in both sexes of MRL/lpr mice. Therefore, IL-1 family signaling, including that of IL-36R, was upregulated in MRL/lpr mice.

4. Discussion

The present study demonstrated the localization of the IL-36 subfamily in murine kidneys (Table 3). In regard to mRNA expression, both sexes of MRL/lpr mice manifested autoimmune nephritis, and our results demonstrated that IL-36α coded by *Il1f6* was the most overexpressed in the kidneys of MRL/lpr mice among the IL-1 family members at the late stage as previously reported (Ichii et al. 2010, 2017). In contrast, no common alteration was observed in the mRNA expression of other IL-36 subfamily members between male and female MRL/lpr mice. In our previous study, murine kidney injury models created by UUO and folic acid injection revealed the downregulation of *Il1f5* and *Il1f8* in the kidney, while Nishikawa *et al*. reported that the mRNA expression of IL-36α, IL-36β, and IL-36γ was upregulated in murine kidneys with ischemia-reperfusion injury (Ichii et al. 2017; Nishikawa et al. 2018). Importantly, a disease-specific expression pattern of the IL-36 subfamily was also reported in other organs. In mice, collagen-induced arthritis increased the mRNA levels of all members of this family; however, only *Il1f6*, *Il1f9*, and *Il1f5* were upregulated in antigen-induced arthritis (Boutet et al. 2016). Thus, these gene expression analyses indicated that IL-36α contributes to the progression of various kidney diseases, while the expression of other members may depend upon disease type.

We investigated the localization of IL-36 subfamily cytokines, and IL-36α was mainly localized to TECs in DT and not in PT. Characteristically, some IL-36α^{+} TECs exhibited

476 decreased specific marker expression for each renal tubule, indicating an alternation of
477 morpho-functional phenotypes. Furthermore, PECs also expressed IL-36α during disease
478 progression in MRL/lpr mice, and this was abundant in males. Chi *et al*. reported the presence of
479 IL-36α^{+} PECs in human patients with a pathologic diagnosis of TIL in nephritis or diabetic
480 nephropathy (Chi et al. 2017). Importantly, IL-36α^{+} PECs frequently presented with a cuboidal
481 and not squamous morphology and a positive reaction for CD44, an activated PEC marker. CD44
482 is a glycoprotein involved in cell-cell interactions, cell adhesion, and cell migration (Smeets et al.
483 2009; Berger and Moeller 2014). Furthermore, IL-36α^{+} PEC number is positively correlated with
484 neutrophil infiltration into the glomerulus in MRL/lpr mice. Neutrophil-secreting enzymes,
485 including elastase, cathepsin G, and proteinase 3, play crucial roles in processing and activating
486 IL-36 agonists, thus suggesting that neutrophils in glomeruli are involved in IL-36α production in
487 PECs (Clancy et al. 2017). In mice, female PECs are squamous, while male PECs are composed
488 of squamous to cuboidal cells under the control of sex-hormones. Furthermore, several
489 glomerular lesions, including focal segmental glomerular sclerosis, are more severe in males than
490 they are in females in mice as well as humans (Ahmadizadeh et al. 1984; Schwartzman-Morris
491 and Putterman 2012; Kuppe et al. 2019). Thus, induced IL-36α expression appeared to be
492 associated with the morpho-functional changes of epithelial cells as TECs and PECs and
493 contribute to the pathogenesis of autoimmune nephritis.

In MRL/lpr mouse kidneys, $CD138^+$ plasma cells expressed IL-36β and IL-38, an agonist and antagonist of IL-36 signaling, respectively. Plasma cells produce antibodies in addition to immunosuppressive and pro-inflammatory cytokines such as IL-10 and IL-17, respectively, (Dang et al. 2014). It has been reported that IL-36α, IL-36β, IL-36γ, and IL-36Ra are expressed in plasma cells, indicating that these cells might be one of the main producers of IL-36 subfamily members (Boutet et al. 2016). In another report, IL-$36\beta^+$ plasma cells were observed in the synovium and colonic mucosa of human patients with rheumatoid arthritis and Crohn's disease, respectively, and the number of IL-$36\beta^+$ cells was increased in the former only (Boutet et al. 2016). In contrast, IL-$36\beta^+$ cells were rarely observed in the tubulointerstitium of MRL/lpr mice at the late stage only. Therefore, we concluded that the contribution of IL-36β to the pathogenesis of autoimmune nephritis in MRL/lpr mice was relatively low compared to that of other members.

In contrast, IL-38^+ plasma cells were significantly increased in MRL/lpr mice during the progression of nephritis; however, the mRNA level was not altered. SLE patients possessed high serum levels of IL-38 that were associated with the risk of lupus nephritis and central nervous system lupus (Rudloff et al. 2015). In MRL/lpr mice and another SLE model mouse induced by pristane, IL-38 injection ameliorated skin inflammation and nephritis and reduced proteinuria (Chu et al. 2017; Xu et al. 2020). Additionally, *in vitro* experiments demonstrated that IL-38 inhibited Th17 responses such as the production of IL-17 and IL-22 that were activated by IL-36

signaling (Van De Veerdonk et al. 2012; Chu et al. 2017). In the present study, infiltration of IL-38^{+} plasma cells into the tubulointerstitium was relatively mild compared to that observed in T-cells and in macrophages. However, the IL-38^{+} cell number in the tubulointerstitium exhibited a positive correlation with certain indices for TIL such as IL-36α^{+} tubule number. Therefore, these results indicated that IL-38 was induced by IL-36α upregulation and was involved in TIL as an antagonist.

We found that IL-36γ and IL-36Ra were constitutively expressed in murine kidneys. IL-36γ was localized to sympathetic nerves in the kidney, as observed previously in the intestine. Another study also revealed that IL-36γ was expressed and upregulated in spinal neurons of a mouse model of chronic inflammatory pain induced by injection of complete Freund's adjuvant (Li et al. 2019). However, in the kidney, IL-36γ was also expressed under healthy conditions. Similar to IL-36γ localization, IL-1α, a member of the IL-1 family, is expressed in rat peripheral nerves in accordance with the distribution of noradrenergic innervation of organs such as the colon and pancreas (Bartfai and Schultzberg 1993). Cytokines exert several physiological functions in the nervous system. For example, tumor necrosis factor α is produced by neurons, astrocytes, and microglia and contributes to the development of the hippocampus, ionic homeostasis, and synaptic plasticity and also to the initiation and progression of some neuronal diseases (Park and Bowers 2010). Further investigation is required to elucidate the physiological

functions of IL-36γ in the kidneys through the function of nerves, and these studies should particularly focus on representative sympathetic nerve activity such as the regulation of renal blood flow (Schiller et al. 2017).

Under healthy conditions, IL-36Ra was expressed in smooth muscle cells of the tunica media of arteries and arterioles and was partially absent in the cells with vasculitis in MRL/lpr mice. It has been reported that IL-36Ra was expressed in keratinocytes, in various immune cells such as B-cells, macrophages, and dendritic cells, and in perivascular cells surrounding the fetal blood vessels of human placentas (Southcombe et al. 2015; Queen et al. 2019). Further, blood vessels in the tumor and tonsil of patients with colon carcinoma express IL-36Ra with IL-36γ, and there was a positive correlation between IL-36Ra expression and the upregulation of immune checkpoint markers such as programmed cell death 1, programmed cell death ligand 1, and cytotoxic T-lymphocyte associated protein 4 (Weinstein et al. 2019). Additionally, DT epithelial cells and PECs also expressed IL-36Ra in accordance with IL-36α localization, and both of them were at least partially co-expressed in DT epithelial cells. Therefore, IL-36Ra induction may be associated with IL-36α overexpression in injured or activated renal epithelial cells to regulate inflammation, and this has been reported as a positive correlation between the mRNA and protein levels in synovial tissues of patients with rheumatoid arthritis (Boutet et al. 2016).

Our ISH study revealed that the mRNA of IL-36R, *Il1rl2*, was ubiquitously expressed in

548 murine kidneys. It has been previously reported that IL-36R is expressed in immune and
549 non-immune cells, where the former are dendritic cells, T-cells, and macrophages and the latter
550 are the epithelial cells of renal tubules and bronchioles, keratinocytes, and fibroblasts (Ichii et al.
551 2017; Queen et al. 2019). Additionally, autoimmune nephritis models exhibited induction of
552 *Il1rl2* in renal lesions, including TECs of dilated tubules and proliferative cells, and this induction
553 was markedly present in mesangial cells and PECs. In MRL/lpr mice at the late stage, our
554 microarray analysis and IHC for p-NF-κB showed the upregulation of genes associated with
555 MAPK and NF-κB pathways, which are common to the IL-1 family, including IL-36α (Towne et
556 al. 2004). In IL-36R-expressing cells, these pathways promote inflammatory responses through
557 the production of cytokines and chemokines, including IL-6, IL-8, TNF-α, CXCL1, and CXCL8,
558 suggesting that renal inflammation in MRL/lpr cells was activated by IL-36α (Queen et al. 2019).
559 Reportedly, patients with SLE show high serum levels of IL-36α, IL-36γ, and IL-38 and a
560 low level of IL-36Ra, and peripheral blood mononuclear cells are suspected to be their origin
561 (Rudloff et al. 2015; Mai et al. 2018). However, the levels of these proteins have not yet been
562 investigated in MRL/lpr mice. In mice, systemic autoimmune disease is caused by *lpr* mutation, a
563 defect in the expression of Fas antigen, which is involved in apoptosis of T-cells to eliminate
564 autoreactive cells under normal conditions (Gillette-Ferguson and Sidman 1994). Furthermore,
565 MRL/lpr mice showed increased expression of *Il1b* and *Ifng* in spleens and lymph nodes before

566 the onset of autoimmune disease, suggesting that *lpr* mutation might be associated with the
567 upregulation of cytokines (Lemay et al. 1996). In the kidneys, we considered that the gene
568 mutation might regulate the IL-36 subfamily expression through indirect pathways; the
569 progression of autoimmune disease might induce renal inflammation, leading to overexpression
570 of IL-36α, which exacerbates the symptoms of nephritis.

571 In conclusion, we demonstrated the functional compartmentalization of the IL-36 subfamily
572 in murine kidneys, and each member exhibited constitutive or induced expression. Although
573 further studies are required to elucidate the functions of each member of this family in the kidneys,
574 our results strongly suggest that a balance of IL-36 agonists and antagonists is maintained under
575 health conditions; however, inflammatory conditions cause an IL-36α-dominant imbalance,
576 ultimately leading to deterioration and increased renal pathology. Therefore, redressing the
577 balance, particularly IL-36α inhibition, may play a key role in the development of novel
578 therapeutic strategies targeting kidney disease.

579

Consent to participate

Author contributions

Ta.N., O.I., Y.O., and Y.K. designed the study; Ta.N., O.I., Te.N., M.A.M., Y.O., M.H., and E.Y.H.A. performed experiments and analyzed the data; Ta.N., O.I., and Y.K. drafted and revised the manuscript. All authors were involved in the writing of the manuscript and approved the final manuscript.

Conflict of interest

The authors have no conflicts of interest directly relevant to the content of this article.

Funding

This study was supported in part by JSPS KAKENHI (grant numbers JP20J22559 [Mr. Namba], 18H02331 and 19K22352 [Dr. Ichii]).

Ethical approval

All animal experiments were approved by the Institutional Animal Care and Use Committee of Hokkaido University and the Faculty of Veterinary Medicine, Hokkaido University (approval No. 16-0024, 20-0012). Our animal experiments program was approved by the Association for

598 Assessment and Accreditation of Laboratory Animal Care International.

Reference

Ahmadizadeh M, Echt R, Chao-Hen K, Hook JB (1984) Sex and strain differences in mouse kidney: Bowman's capsule morphology and susceptibility to chloroform. Toxicol Lett 20:161–171. https://doi.org/10.1016/0378-4274(84)90142-5

Ahsan F, Maertzdorf J, Guhlich-Bornhof U, Kaufmann SHE, Moura-Alves P (2018) IL-36/LXR axis modulates cholesterol metabolism and immune defense to Mycobacterium tuberculosis. Sci Rep 8:1520. https://doi.org/10.1038/s41598-018-19476-x

Almaani S, Meara A, Rovin BH (2017) Update on lupus nephritis. Clin J Am Soc Nephrol 12:825–835. https://doi.org/10.2215/CJN.05780616

Bartfai T, Schultzberg M (1993) Cytokines in neuronal cell types. Neurochem Int 22:435–444. https://doi.org/10.1016/0197-0186(93)90038-7

Berger K, Moeller MJ (2014) Mechanisms of epithelial repair and regeneration after acute kidney injury. Semin Nephrol 34:394–403. https://doi.org/10.1016/j.semnephrol.2014.06.006

Blumberg H, Dinh H, Dean C, Trueblood ES, Bailey K, Shows D, Bhagavathula N, Aslam MN, Varani J, Towne JE, Sims JE (2010) IL-1RL2 and Its Ligands Contribute to the Cytokine Network in Psoriasis. J Immunol 185:4354–4362. https://doi.org/10.4049/jimmunol.1000313

Blumberg H, Dinh H, Trueblood ES, Pretorius J, Kugler D, Weng N, Kanaly ST, Towne JE, Willis CR, Kuechle MK, Sims JE, Peschon JJ (2007) Opposing activities of two novel members of the IL-1 ligand family regulate skin inflammation. J Exp Med 204:2603–2614. https://doi.org/10.1084/jem.20070157

Boutet MA, Bart G, Penhoat M, Amiaud J, Brulin B, Charrier C, Morel F, Lecron JC, Rolli-Derkinderen M, Bourreille A, Vigne S, Gabay C, Palmer G, Le Goff B, Blanchard F (2016) Distinct expression of interleukin (IL)-36α, β and γ, their antagonist IL-36Ra and

623 IL-38 in psoriasis, rheumatoid arthritis and Crohn's disease. Clin Exp Immunol 184:159–
624 173. https://doi.org/10.1111/cei.12761
625 Chen TK, Knicely DH, Grams ME (2019) Chronic Kidney Disease Diagnosis and Management:
626 A Review. JAMA - J Am Med Assoc 322:1294–1304.
627 https://dx.doi.org/10.1001%2Fjama.2019.14745
628 Chi H-H, Hua K-F, Lin Y-C, Chu C-L, Hsieh C-Y, Hsu Y-J, Ka S-M, Tsai Y-L, Liu F-C, Chen A
629 (2017) IL-36 Signaling Facilitates Activation of the NLRP3 Inflammasome and
630 IL-23/IL-17 Axis in Renal Inflammation and Fibrosis. J Am Soc Nephrol 28:2022–2037.
631 https://doi.org/10.1681/ASN.2016080840
632 Chu M, Tam LS, Zhu J, Jiao D, Liu DH, Cai Z, Dong J, Kai Lam CW, Wong CK (2017) In vivo
633 anti-inflammatory activities of novel cytokine IL-38 in Murphy Roths Large (MRL)/lpr
634 mice. Immunobiology 222:483–493. https://doi.org/10.1016/j.imbio.2016.10.012
635 Chu M, Wong CK, Cai Z, Dong J, Jiao D, Kam NW, Lam CWK, Tam LS (2015) Elevated
636 expression and pro-inflammatory activity of IL-36 in patients with systemic lupus
637 erythematosus. Molecules 20:19588–19604. https://doi.org/10.3390/molecules201019588
638 Clancy DM, Henry CM, Sullivan GP, Martin SJ (2017) Neutrophil extracellular traps can serve as
639 platforms for processing and activation of IL-1 family cytokines. FEBS J 284:1712–1725.
640 https://doi.org/10.1111/febs.14075
641 Cohen PL, Eisenberg RA (1991) *Lpr* and *gld* : Single Gene Models of Systemic Autoimmunity
642 and Lymphoproliferative Disease. Annu Rev Immunol 9:243–269.
643 https://doi.org/10.1146/annurev.iy.09.040191.001331
644 Dang VD, Hilgenberg E, Ries S, Shen P, Fillatreau S (2014) From the regulatory functions of B
645 cells to the identification of cytokine-producing plasma cell subsets. Curr Opin Immunol
646 28:77–83. https://doi.org/10.1016/j.coi.2014.02.009

647 Garlanda C, Dinarello CA, Mantovani A (2013) The Interleukin-1 Family: Back to the Future.
648 Immunity 39:1003–1018. https://dx.doi.org/10.1016%2Fj.immuni.2013.11.010
649 Gillette-Ferguson I, Sidman CL (1994) A specific intercellular pathway of apoptotic cell death is
650 defective in the mature peripheral T cells of autoimmune *lpr* and *gld* mice. Eur J Immunol
651 24:1181–1185. https://doi.org/10.1002/eji.1830240526
652 Ichii O, Kimura J, Okamura T, Horino T, Nakamura T, Sasaki H, Elewa YHA, Kon Y (2017)
653 IL-36α Regulates Tubulointerstitial Inflammation in the Mouse Kidney. Front Immunol
654 8:1346. https://doi.org/10.3389/fimmu.2017.01346
655 Ichii O, Otsuka S, Sasaki N Yabuki A, Ohta H, Takiguchi M, Hashimoto Y, Endoh D, Kon Y
656 (2010) Local overexpression of interleukin-1 family, member 6 relates to the development
657 of tubulointerstitial lesions. Lab Investig 90:459–475.
658 https://doi.org/10.1038/labinvest.2009.148
659 Iwata Y, Furuichi K, Kaneko S, Wada T (2011) The role of cytokine in the lupus nephritis. J
660 Biomed Biotechnol 2011: 594809. https://doi.org/10.1155/2011/594809
661 Johnston A, Xing X, Guzman AM, Riblett M, Loyd CM, Ward NL, Wohn C, Prens EP, Wang F,
662 Maier LE, Kang S, Voorhees JJ, Elder JT, Gudjonsson JE (2011) IL-1F5, -F6, -F8, and -F9:
663 A Novel IL-1 Family Signaling System That Is Active in Psoriasis and Promotes
664 Keratinocyte Antimicrobial Peptide Expression. J Immunol 186:2613–2622.
665 https://doi.org/10.4049/jimmunol.1003162
666 Kuppe C, Leuchtle K, Wagner A, Kabgani N, Saritas T, Puelles VG, Smeets B, Hakroush S, van
667 der Vlag J, Boor P, Schiffer M, Gröne HJ, Fogo A, Floege J, Moeller MJ (2019) Novel
668 parietal epithelial cell subpopulations contribute to focal segmental glomerulosclerosis and
669 glomerular tip lesions. Kidney Int 96:80–93. https://doi.org/10.1016/j.kint.2019.01.037
670 Lemay S, Mao C, Singh AK (1996) Cytokine gene expression in the MRL/lpr model of lupus

671 nephritis. Kidney Int 50:85–93. https://doi.org/10.1038/ki.1996.290
672 Li Q, Liu S, Li L, Ji X, Wang M, Zhou J (2019) Spinal IL-36γ/IL-36R participates in the
673 maintenance of chronic inflammatory pain through astroglial JNK pathway. Glia 67:438–
674 451. https://doi.org/10.1002/glia.23552
675 Mai S Z, Li C J, Xie X Y, Xiong H, Xu M, Zeng F Q, Guo Q, Han Y F (2018) Increased serum
676 IL-36α and IL-36γ levels in patients with systemic lupus erythematosus: Association with
677 disease activity and arthritis. Int Immunopharmacol 58:103–108.
678 https://doi.org/10.1016/j.intimp.2018.03.011
679 Mantovani A, Dinarello CA, Molgora M, Garlanda C (2019) Interleukin-1 and Related Cytokines
680 in the Regulation of Inflammation and Immunity. Immunity 50:778–795.
681 https://doi.org/10.1016/j.immuni.2019.03.012
682 Milora KA, Fu H, Dubaz O, Jensen LE (2015) Unprocessed interleukin-36α regulates
683 psoriasis-like skin inflammation in cooperation with interleukin-1. J Invest Dermatol
684 135:2992–3000. https://doi.org/10.1038/jid.2015.289
685 Nishikawa H, Taniguchi Y, Matsumoto T, Arima N, Masaki M, Shimamura Y, Inoue K, Horino T,
686 Fujimoto S, Ohko K, Komatsu T, Udaka K, Sano S, Terada Y (2018) Knockout of the
687 interleukin-36 receptor protects against renal ischemia-reperfusion injury by reduction of
688 proinflammatory cytokines. Kidney Int 93:599–614.
689 https://doi.org/10.1016/j.kint.2017.09.017
690 Park KM, Bowers WJ (2010) Tumor necrosis factor-alpha mediated signaling in neuronal
691 homeostasis and dysfunction. Cell. Signal. 22:977–983.
692 https://dx.doi.org/10.1016%2Fj.cellsig.2010.01.010
693 Queen D, Ediriweera C, Liu L (2019) Function and Regulation of IL-36 Signaling in
694 Inflammatory Diseases and Cancer Development. Front Cell Dev Biol 7:317.

https://dx.doi.org/10.3389%2Ffcell.2019.00317

Ramesh G, Reeves WB (2004) Inflammatory cytokines in acute renal failure. Kidney Int. Suppl. 66:S56–S61. https://doi.org/10.1111/j.1523-1755.2004.09109.x

Rudloff I, Godsell J, Nold-Petry CA, Harris J, Hoi A, Morand EF, Nold MF (2015) Brief Report: Interleukin-38 Exerts Antiinflammatory Functions and Is Associated With Disease Activity in Systemic Lupus Erythematosus. Arthritis Rheumatol 67:3219–3225. https://doi.org/10.1002/art.39328

Schiller AM, Pellegrino PR, Zucker IH (2017) Eppur Si Muove: The dynamic nature of physiological control of renal blood flow by the renal sympathetic nerves. Auton Neurosci Basic Clin 204:17–24. https://doi.org/10.1016/j.autneu.2016.08.003

Schwartzman-Morris J, Putterman C (2012) Gender differences in the pathogenesis and outcome of lupus and of lupus nephritis. Clin Dev Immunol 2012:604892. https://dx.doi.org/10.1155%2F2012%2F604892

Smeets B, Uhlig S, Fuss A, Mooren F, Wetzels JFM, Floege J, Moeller MJ (2009) Tracing the origin of glomerular extracapillary lesions from parietal epithelial cells. J Am Soc Nephrol 20:2604–2615. https://doi.org/10.1681/ASN.2009010122

Southcombe JH, Redman CWG, Sargent IL, Granne I (2015) Interleukin-1 family cytokines and their regulatory proteins in normal pregnancy and pre-eclampsia. Clin Exp Immunol 181:480–490. https://doi.org/10.1111/cei.12608

Towne JE, Garka KE, Renshaw BR, Virca GD, Sims JE (2004) Interleukin (IL)-1F6, IL-1F8, and IL-1F9 Signal Through IL-1Rrp2 and IL-1RAcP to Activate the Pathway Leading to NF-κB and MAPKs. J Biol Chem 279:13677–13688. https://doi.org/10.1074/jbc.M400117200

Van De Veerdonk FL, Stoeckman AK, Wu G, Boeckermann AN, Azam T, Netea MG, Joosten LAB, Van Der Meer JWM, Hao R, Kalabokis V, Dinarello CA (2012) IL-38 binds to the

IL-36 receptor and has biological effects on immune cells similar to IL-36 receptor antagonist. Proc Natl Acad Sci USA 109:3001–3005. https://doi.org/10.1073/pnas.1121534109

Webster AC, Nagler E V., Morton RL, Masson P (2017) Chronic Kidney Disease. Lancet 389:1238–1252. https://doi.org/10.1016/S0140-6736(16)32064-5

Weinstein AM, Giraldo NA, Petitprez F, Julie C, Lacroix L, Peschaud F, Emile JF, Marisa L, Fridman WH, Storkus WJ, Sautès-Fridman C (2019) Association of IL-36γ with tertiary lymphoid structures and inflammatory immune infiltrates in human colorectal cancer. Cancer Immunol Immunother 68:109–120. https://doi.org/10.1007/s00262-018-2259-0

Xu W D, Su L C, Liu X Y, Wang J M, Yuan Z C, Qin Z, Zhou X P, Huang A F (2020) IL-38: A novel cytokine in systemic lupus erythematosus pathogenesis. J Cell Mol Med jcmm. 24: 12379-12389. https://doi.org/10.1111/jcmm.15737

Yu C, Gershwin ME, Chang C (2014) Diagnostic criteria for systemic lupus erythematosus: A critical review. J Autoimmun 48–49:10–13. https://doi.org/10.1016/j.jaut.2014.01.004

Figure Legends

Figure 1. mRNA expression of IL-36 subfamily members in the murine kidneys

(a-e) Relative mRNA expression of IL-36 subfamily members in the kidneys. The expression levels are normalized to the values of beta-actin (*Actb*) of female MRL/+ mice at the early stage of autoimmune nephritis. Each bar represents the mean ± SE (n= 4-11). *: Significant difference in MRL/lpr mice against MRL/+ mice of the same sex at the same stage (*: $P < 0.05$, **: $P < 0.01$). †: Significant difference in female against male mice of the same strain at the same stage (†: $P < 0.05$, ††: $P < 0.01$). §: Significant difference at the late stage against the early stage in the same mice strains of the same sex (§: $P < 0.05$, §§: $P < 0.01$). Mann-Whitney *U*-test. F: Female. M: Male. Early: Early stage of autoimmune nephritis (3 months). Late: Late stage of autoimmune nephritis (6-7 months). Quantitative PCR analysis.

Figure 2. IL-36α localization in the renal tubules of the murine kidneys

(a-b''') Immunohistochemistry (IHC) images for IL-36α. IL-36α^{+} renal tubules (arrowheads) are observed in all groups at the early stage of autoimmune nephritis, and those numbers tends to increase in both sexes of MRL/lpr mice as they age. Meanwhile, IL-36α^{+} renal corpuscles (arrows) are frequently found in male MRL/lpr mice at the late stage. Bars= 100 μm.

(c and c') Representative IHC images for IL-36α in male MRL/lpr mice at the early and late stages.

753 IL-36α^{+} reactions (arrowheads) are observed in the cytoplasm and nucleus of tubular epithelial
754 cells, including a segment of macula densa (MD) and dilated tubules with urinary cast. Bars= 50
755 μm.
756 (d) The number of IL-36α^{+} renal tubules. Each bar represents the mean ± SE (n= 4-9). *:
757 Significant difference in MRL/lpr against MRL/+ mice of the same sex at the same stage (*: $P <$
758 0.05). †: Significant difference in female against male mice of the same strain at the same stage
759 (†: $P < 0.05$). §: Significant difference at the late stage against the early stage in the same mouse
760 strains of the same sex (§: $P < 0.05$, §§: $P <0.01$). Mann-Whitney *U*-test.
761 (e-f") Representative double immunofluorescence images for IL-36α (green) with
762 calbindin-D28k (red, distal tubule marker) or HNF-4α (red, proximal tubule marker) in male
763 MRL/lpr mice at the late stage. IL-36α^{+} cells are mainly observed in calbindin-D28k^{+} distal
764 tubules (panel e-e"), while the number of these cells in HNF-4α^{+} proximal tubules is quite few
765 (panel f-f"). Arrowheads indicate IL-36α^{+}, calbindin-D28k^{+}, or HNF-4α^{+} cells. The nucleus is
766 stained by Hoechst (blue). Insets indicate high magnification images of areas marked by the white
767 squares. Bars= 50 μm.
768 F: Female. M: Male. Early: Early stage of autoimmune nephritis (3 months). Late: Late stage of
769 autoimmune nephritis (6-7 months).
770

Figure 3. IL-36α localization in parietal epithelial cells of the murine kidneys

(a and a') Representative immunohistochemistry images for IL-36α in female and male MRL/lpr mice at the late stage of autoimmune nephritis. IL-36α^{+} reactions (arrowheads) are observed in the cytoplasm and nucleus of cuboidal parietal epithelial cells (PECs). Bars= 50 μm.

(b) Percentage of the number of IL-36α^{+} renal corpuscles (RCs) to that of total RCs. Each bar represents the mean ± SE (n= 4-9). *: Significant difference in MRL/lpr against MRL/+ mice of the same sex at the same stage (**: P <0.01). †: Significant difference in female against male mice of the same strain at the same stage (†: P < 0.05, ††: P <0.01). §: Significant difference at the late stage against the early stage in the same mouse strains of the same sex (§§: P <0.01). Mann-Whitney *U*-test. ND: Not detected.

(c-c") Representative double immunofluorescence images for IL-36α (green) and CD44 (red) in male MRL/lpr mice at the late stage. IL-36α is frequently co-expressed in CD44^{+} PECs (arrowheads). Arrows indicate infiltrated CD44^{+} cells. The nucleus is stained by Hoechst (blue). Inset indicates high magnification image of area marked by the white square. Bars= 50 μm.

(d) Percentage of IL-36α^{+} PECs in CD44 positive and negative PECs in male MRL/lpr mice at the late stage. Each bars represent the mean ± SE (n= 5). *: Significant difference in CD44^{+} PECs against CD44^{-} PECs (Mann-Whitney *U*-test, ** P < 0.01).

F: Female. M: Male. Early: Early stage of autoimmune nephritis (3 months). Late: Late stage

789 autoimmune nephritis (6-7 months).

790

791 **Figure 4. Localization of IL-36β and IL-36γ in murine kidneys**

792 (a) Representative immunohistochemistry (IHC) image for IL-36β in female MRL/lpr mice at the

793 late stage of autoimmune nephritis. IL-36β^+ reactions (arrowheads) are rarely observed in the

794 cytoplasm of interstitial cells. Bars= 50 μm.

795 (b-b") Representative double immunofluorescence (IF) images for IL-36β (green) and CD138

796 (red, plasma cell marker) in female MRL/lpr mice at the late stage. IL-36β is expressed in CD138$^+$

797 plasma cells (arrowheads). Arrows indicate IL-36β^- CD138$^+$ cells. The nucleus is stained by

798 Hoechst (blue). Inset indicates high magnification image of the area marked by the white square.

799 Bars= 50 μm.

800 (c) Representative IHC image for IL-36γ in male MRL/lpr mice at the late stage. IL-36γ^+

801 reactions (arrowheads) are found mainly in the interstitium surrounding the vessels or renal

802 corpuscles. Bars= 50 μm.

803 (d-d") Representative double IF images for IL-36γ (green) and tyrosine hydroxylase (red,

804 sympathetic nerve marker) in male MRL/+ mice at the late stage. Tyrosine hydroxylase$^+$

805 sympathetic axons exhibit IL-36γ positive and negative reactions (arrowheads and arrows,

806 respectively). The nucleus is stained by Hoechst (blue). Inset indicates high magnification image

807 of the area marked by the white square. Bars= 50 μm.

808 F: Female. M: Male. Late: Late stage autoimmune nephritis (6-7 months).

809

810 **Figure 5. Localization of IL-36Ra in the murine kidneys**

811 (a) Representative immunohistochemistry (IHC) image for IL-36Ra in male MRL/lpr mice at the

812 late stage of autoimmune nephritis. IL-36Ra^{+} reactions (arrowheads) are observed in the tunica

813 media of arteries. IA: Interlobar artery. AA: Arcuate artery. L: Lumen of renal pelvis. Bars= 100

814 μm.

815 (b-b") Representative double immunofluorescence (IF) images for IL-36Ra (green) with

816 alpha-smooth muscle actin (α-SMA; red, smooth muscle cell marker) in male MRL/lpr mice at

817 the late stage. IL-36Ra^{+} reactions are observed in the cytoplasm of smooth muscle cells of arteries

818 and arterioles. Arrowheads indicate IL-36Ra^{+} or α-SMA^{+} cells. The nucleus is stained by Hoechst

819 (blue). Dotted lines represent renal corpuscles. Inset indicates high magnification image of the

820 area marked by the white square. InA: Intralobular artery. GA: Glomerular arteriole. Bars= 50

821 μm.

822 (c-e) Representative IHC images for IL-36Ra in male MRL/lpr mice at the late stage. The

823 IL-36Ra^{+} reaction in smooth muscle cells with vasculitis (asterisk) is partially defective (panel c).

824 IL-36Ra^{+} reactions are observed in parietal and tubular epithelial cells (panel d and e,

825 respectively). Arrowheads indicate IL-36Ra$^+$ reactions. Insets indicate high magnification images

826 of the areas marked by the black squares. IA: Interlobar artery. Bars= 50 μm.

827 (f-f'') Representative double IF images for IL-36Ra (green) and calbindin-D28k (red, distal tubule

828 marker) in male MRL/lpr mice at the late stage. The granular IL-36Ra$^+$ reactions are expressed in

829 the apical portion of distal tubular epithelial cells. Arrowheads indicate IL-36Ra$^+$ or

830 calbindin-D28k$^+$ cells. The nucleus is stained by Hoechst (blue). Insets indicate high

831 magnification images of areas marked by the black squares. Bars= 50 μm.

832 (g and g') Representative serial sections followed by IHC for IL-36Ra and HNF-4α (proximal

833 tubule marker) in male MRL/lpr mice at the late stage. The IL-36Ra$^+$ reaction is not observed in

834 HNF-4α$^+$ proximal tubules. Asterisks indicate IL-36Ra$^+$ HNF-4α$^-$ tubules. Bars= 50 μm.

835 (h and h') Representative serial sections followed by IHC for IL-36Ra and IL-36α in female

836 MRL/lpr mice at the late stage. A portion of the tubular epithelial cells co-express IL-36Ra and

837 IL-36α (arrowheads). Asterisks indicate the same tubules. Insets indicate high magnification

838 images of the areas marked by the black squares. Bars= 50 μm.

839 F: Female. M: Male. Late: Late stage autoimmune nephritis (6-7 months).

840

841 **Figure 6. Localization of IL-38 in the murine kidneys**

842 (a-b''') Immunohistochemistry (IHC) images for IL-38. IL-38$^+$ cells are found in the

tubulointerstitium of all groups, and that number is abundant in both sexes of MRL/lpr mice at late stage of autoimmune nephritis compared to those observed in the others. Bars= 50 μm.

(c and c') Representative serial sections followed by IHC for IL-38 and CD138 (plasma cell marker) in male MRL/lpr mice at the late stage. IL-38 is expressed in $CD138^+$ plasma cells (arrowheads). Bars= 50 μm.

(d) The number of $IL\text{-}38^+$ cells in the tubulointerstitium. Each bar represents the mean ± SE (n= 4-9). §: Significant difference at the late stage against the early stage in the same mouse strains of same sex (§: $P < 0.05$). Mann-Whitney *U*-test.

(e and e') Representative serial sections followed by IHC for IL-38 and IL-36α in female MRL/lpr mice at the late stage. $IL\text{-}38^+$ cells (arrowheads) are not surrounding $IL\text{-}36\alpha^+$ renal tubules (asterisks). Bars= 50 μm.

F: Female. M: Male. Early: Early stage of autoimmune nephritis (3 months). Late: Late stage autoimmune nephritis (6-7 months).

Figure 7. *Il1rl2* localization and upregulated downstream-genes involved in IL-1 family signaling in murine kidneys

(a-b''') Representative *in situ* hybridization (ISH) images for *Il1rl2* in male MRL/+ and MRL/lpr mice at the late stage of autoimmune nephritis. $Il1rl2^+$ reactions (arrowheads) are observed in

glomeruli, tubulointerstitium, and vasculature from cortex to medulla in both strains, and this expression is induced in glomerular and tubulointerstitial lesions of MRL/lpr mice. Dotted lines indicate renal corpuscles (RCs). Insets indicate high magnification images of the areas marked by the black squares. Ti: Tubulointerstitium. L: Lumen of renal pelvis. Bars= 50 μm.

(c and c') Representative ISH for *Il1rl2* images followed by periodic acid Schiff-hematoxylin (PAS-H) staining in female MRL/lpr mice at the late stage. *Il1rl2*$^{+}$ reaction (arrowheads) is observed in PAS^{-} distal tubules (DTs) and not in PAS^{+} proximal tubules (PTs). The positive cells are in close proximity to the vascular pole in MRL/lpr mice at the late stage. Insets indicate high magnification images of the areas marked by the black squares. MD: Macula densa. Bars= 50 μm.

(d) mRNA expression of *Il1rl2* coding IL-36R in kidneys. The expression levels are normalized to the values of beta-actin (*Actb*), and those of female MRL/+ mice at the early stage. Each bar represents the mean ± SE (n= 4-11).

(e and f) Gene ontology (GO) analysis for positive regulation of mitogen-activated protease (MAPK) activity (GO: 0043406; panel e) and of nuclear factor kappa B (NF-κB) transcription factor activity (GO: 0051092; panel f) in the kidneys of female MRL/lpr mice at the late stage compared to those values in female MRL/+ mice at the same stage. MRL/lpr mice possess 25 genes associated with positive regulation of MAPK activity (panel e) and 11 genes associated NF-κB transcription factor activity (panel f) that are upregulated more than 2-fold compared to

879 those of MRL/+ mice. Each value represents the relative mRNA level of MRL/lpr mice against
880 MRL/+ mice (n =3). *: Significant difference in female MRL/lpr mice at the late stage against the
881 same sexes of MRL/+ mice at the same stage (Student t-test, * $P < 0.05$, ** $P < 0.01$). Min:
882 Minimum expression of mRNA in the list. Max: Maximum expression of mRNA in the list.
883 F: Female. M: Male. Early: Early stage of autoimmune nephritis (3 months). Late: Late stage
884 autoimmune nephritis (6-7 months).
885

Table 1. Indices of autoimmune disease, renal functions, and renal histopathology

		Early				Late			
		Female		Male		Female		Male	
	Index	MRL/+	MRL/lpr	MRL/+	MRL/lpr	MRL/+	MRL/lpr	MRL/+	MRL/lpr
Autoimmune disease	S/B ratio (%)	0.26 ± 0.01[b*]	0.69 ± 0.07[a*]	0.20 ± 0.01	0.59 ± 0.08[a*]	0.25 ± 0.02	2.29 ± 0.53[a**,c**]	0.22 ± 0.01	1.54 ± 0.23[a**,c*]
	dsDNA (U/mL)	7.56 ± 0.94	406.31 ± 74.99[a*]	3.77 ± 1.58	201.71 ± 39.23[a*]	8.70 ± 3.95	807.90 ± 88.02[a*]	11.46 ± 3.67	632.48 ± 95.29[a**,c**]
Renal function	BUN (mg/dL)	20.83 ± 2.14	28.23 ± 5.42	28.28 ± 1.77	31.93 ± 4.97	26.60 ± 2.08	52.63 ± 3.33[a*]	21.13 ± 1.64	36.81 ± 4.53[a*]
	Cr (mg/dL)	0.38 ± 0.06	0.28 ± 0.03	0.34 ± 0.10	0.32 ± 0.04	0.29 ± 0.06	0.51 ± 0.15	0.70 ± 0.39	1.13 ±0.80
	uACR (μg/mg)	NE				29.40 ± 10.43[§]	345.021 ± 133.42	42.03 ± 9.94	463.14 ± 118.14
Renal histopathology	Glo. Nucleus (No.)	41.95 ± 0.41	45.4 ± 0.20[a*,b*]	42.33 ± 1.11	47.63 ± 0.54[a*]	45.65 ± 0.96[§]	78.64 ± 5.59[a**,c**]	43.08 ± 0.37	62.74 ± 5.13[a**,c*]
	Glo. Size (×10^3 μm^2)	2.18 ± 0.03[b*]	2.24 ± 0.07[b*]	2.54 ± 0.05	2.82 ± 0.10[a*]	2.94 ± 0.19[†§]	5.54 ± 0.63[a**,c**]	2.58 ± 0.03	4.51 ± 0.42[a**,c*]
	Mesangial area (%)	34.89 ± 1.07	40.10 ± 0.79[a*]	36.23 ± 0.95	38.61 ± 0.74[a*]	37.33 ± 1.40[§]	47.08 ± 2.17[a*,b*,c*]	34.32 ± 0.88	46.10 ± 1.92[a**]
	Glo. B220 (No./Glo.)	0.03 ± 0.02	0.03 ± 0.03	0.03 ± 0.02	0.08 ± 0.02	0.03 ± 0.02	1.46 ± 0.43[a**,c**]	0.08 ± 0.03	0.90 ± 0.17[a**,c**]
	Glo. CD3 (No./Glo.)	0.11 ± 0.03	0.18 ± 0.06	0.10 ± 0.04	0.17 ± 0.04	0.11 ± 0.03	1.95 ± 0.38[a**,c**]	0.13 ± 0.02	1.21 ± 0.23[a**,c**]
	Glo. Iba-1 (No./Glo.)	0.01 ± 0.01	0.02 ± 0.01	0.01 ± 0.01	0.12 ± 0.06	0.17 ± 0.13	1.65 ± 0.18[a*,c**]	0.03 ± 0.02	0.74 ± 0.10[a**,c**]
	Glo. Gr-1 (No./Glo.)	0.11 ± 0.02	0.12 ± 0.04	0.09 ± 0.05	0.21 ± 0.08	0.28 ± 0.13[†]	0.81 ± 0.10[a*,c**]	0.13 ± 0.03	1.03 ± 0.31[a**,c*]
	Ti. B220 (No./mm^2)	5.42 ± 2.19	10.38 ± 2.78	7.08 ± 2.20	13.92 ± 2.99	10.38 ± 3.49	52.70 ± 11.04[a*,c**]	14.15 ± 1.76	45.60 ± 4.05[a**,c**]
	Ti. CD3 (No./mm^2)	13.21 ±1.72	93.16 ± 1.56[a*]	23.35 ± 4.08	86.79 ± 3.11[a*]	24.76 ± 10.29	296.43 ± 32.25[a**,c**]	40.33 ± 4.45[c*]	196.22 ±27.35[a**,c**]
	Ti. Iba-1 (No./mm^2)	3.99 ± 1.42	26.52 ± 6.42[a*]	17.34 ± 14.16	38.28 ± 10.67	127.12 ± 21.46[§]	386.15 ± 50.66[a**,c**]	159.20 ± 11.71[c*]	289.18 ± 21.88[a**,c**]
	Ti. Gr-1 (No./mm^2)	2.83 ± 1.02	7.55 ± 1.85	3.77 ± 0.39	9.43 ± 1.02[a*]	13.21 ± 4.92[§]	23.46 ± 2.58[a*,c*]	14.39 ± 1.05[c*]	20.21 ± 2.33[a*,c**]

Each value represents the mean ± SE (n = 4–9, except for Cr; n = 3–8). Mann–Whitney *U* test

S/B ratio weight ratio of spleen to body, *dsDNA* serum anti-double-stranded DNA antibody level, *BUN* blood urea nitrogen, *Cr* serum creatinine level, *uACR* urinary albumin-to-creatinine ratio, *Glo* glomerulus, *Ti* tubulointerstitium, *No* number, *NE* not examined, *Early* early stage autoimmune nephritis (3 months), *Late* late stage autoimmune nephritis (6–7 months)

[a]Significant difference in MRL/lpr against MRL/ + mice of the same sex at the same stage (*$P < 0.05$, **$P < 0.01$)

[b]Significant difference in female versus male mice of the same strain at the same stage (*$P < 0.05$, **$P < 0.01$)

[c]Significant difference at the late stage against the early stage in the same mouse strains of the same sex (*$P < 0.05$, **$P < 0.01$)

Table 2. Correlation analysis between parameters of IL-36α and IL-38 and indices for autoimmune nephritis in MRL/lpr

Index		IL36α⁺ tubules				IL36α⁺ PECs				Ti. IL-38⁺ cells			
		Female		Male		Female		Male		Female		Male	
		ρ	*P*	ρ	*P*	ρ	*P*	ρ	*P*	ρ	*P*	ρ	*P*
Autoimmune disease	S/B ratio	0.500	0.117	0.681*	0.010	0.121	0.722	0.736**	<0.010	0.401	0.222	0.391	0.187
	dsDNA	0.782**	<0.010	0.698**	<0.010	0.528	0.117	0.714**	<0.010	0.646*	0.044	0.624*	0.023
Renal function	BUN	0.636*	0.035	0.413	0.161	0.674*	0.023	0.487	0.091	0.668*	0.025	0.157	0.608
	Cr	0.517	0.126	-0.191	0.573	0.429	0.215	0.036	0.915	0.633*	0.050	-0.014	0.968
	uACR	0.943**	<0.010	0.967**	<0.010	0.845*	0.034	0.800*	0.010	0.671*	0.034	0.680*	0.011
Renal histopathology	Glo. Nucleus	0.927**	<0.010	0.791**	<0.010	0.674*	0.023	0.923**	<0.010	0.691*	0.018	0.737**	<0.010
	Glo. Size	0.918**	<0.010	0.819**	<0.010	0.674*	0.023	0.918**	<0.010	0.807**	<0.010	0.770**	<0.010
	Mesangial area	0.818**	<0.010	0.791**	<0.010	0.661*	0.027	0.709**	<0.010	0.673*	0.023	0.704**	<0.010
	Glo. B220⁺ cells	0.615*	0.044	0.736**	<0.010	0.122	0.720	0.711**	<0.010	0.474	0.140	0.415	0.158
	Glo. CD3⁺ cells	0.659*	0.027	0.797**	<0.010	0.231	0.495	0.758**	<0.010	0.480	0.135	0.523	0.067
	Glo. Iba-1⁺ cells	0.548	0.081	0.865**	<0.010	0.190	0.577	0.901**	<0.010	0.375	0.256	0.728**	<0.010
	Glo. Gr-1⁺ cells	0.888**	<0.010	0.802**	<0.010	0.676*	0.022	0.906**	<0.010	0.624*	0.040	0.632*	0.021
	Ti. B220⁺ cells	0.718*	0.013	0.652*	0.016	0.283	0.399	0.465	0.109	0.636*	0.035	0.277	0.360
	Ti. CD3⁺ cells	0.918**	<0.010	0.857**	<0.010	0.674*	0.023	0.758**	<0.010	0.880**	<0.010	0.597*	0.031
	Ti. Iba-1⁺ cells	0.900**	<0.010	0.808**	<0.010	0.674*	0.023	0.648*	0.017	0.737**	0.010	0.370	0.208
	Ti. Gr-1⁺ cells	0.679*	0.022	0.731**	<0.010	0.392	0.233	0.736**	<0.010	0.610*	0.046	0.404	0.171
	IL-36α⁺ tubules	-	-	-	-	0.674*	0.023	0.885**	<0.010	0.820**	<0.010	0.737**	<0.010
	IL-36α⁺ PECs	0.674*	0.023	0.885**	<0.010	-	-	-	-	0.547	0.082	0.779**	<0.010
	Ti. IL-38⁺ cells	0.820**	<0.010	0.737**	<0.010	0.547	0.082	0.779**	<0.010	-	-	-	-

ρ: Spearman's correlation coefficient (n= 6-13, * $P < 0.05$, ** $P < 0.01$). S/B ratio: Weight ratio of spleen to body. dsDNA: Serum anti-double-stranded DNA antibody level. BUN: Blood urea nitrogen Cr: Serum creatinine level uACR: Urinary albumin to creatinine ratio. Glo: Glomerulus. Ti: Tubulointerstitium PECs: Parietal epithelial cells.

Table 3. Localization of IL-36 subfamily members in murine kidneys

	IL-36α	IL-36β	IL-36γ	IL-36Ra	IL-38
TEC	I	-	-	I	-
PEC	I	-	-	I	-
Plasma cell	-	I	-	-	I
Sympathetic axon	-	-	C	-	-
Smooth muscle cell	-	-	-	C	-

I: Inducible expression in autoimmune nephritis. C: Constitutive expression. TEC: Tubular epithelial cell. PEC: Parietal epithelial cell.

Supplemental table 1. Antibodies used in this study

	Antibody	Host	Dilution	Source	Antigen retrieval	Blocking serum	
						IHC	IF
Primary antibody	anti-B220	Rat	1:1600	Cedarlane, Burlington, Canada	Tris 110℃ 15min	10% NGS	
	anti-CD3	Rabbit	1:200	Nichirei, Tokyo, Japan	Tris 110℃ 15min	10% NGS	
	anti-Iba-1	Rabbit	1:1200	Wako, Tokyo, Japan	Tris 110℃ 15min	10% NGS	
	anti-Gr-1	Rat	1:800	R and D system, Minneapolis, MN, USA	Pepsin 37℃ 5min	10% NGS	
	anti-CD138	Rat	1:300	Biolegend, San Diego, CA, USA	Tris 110℃ 15min	10% NGS	5% NDS
	anti-CD44	Rat	1:800	BD Biosciences, Franklin Lakes, NJ, USA	Tris 110℃ 15min		5% NDS
	anti-α-SMA	Rabbit	1:3000	Abcam, Cambridge, UK	Tris 110℃ 15min		5% NDS
	anti-Tyrosine hydroxylase	Rabbit	1:1000	Abcam, Cambridge, UK	Tris 110℃ 15min		5% NDS
	anti-Calbindin-D28k	Rabbit	1:1000	Proteintech, Rosemont, IL, USA	Tris 110℃ 15min		5% NDS
	anti-HNF-4α	Rabbit	1:1000	Cell signaling, Danvers, MA, USA	Tris 110℃ 15min		5% NDS
	anti-IL-36α	Goat	1:400	R and D system, Minneapolis, MN, USA	CB 110℃ 15min	5% NDS	5% NDS
	anti-IL-36β	Goat	1:2000	R and D system, Minneapolis, MN, USA	Tris 110℃ 15min	5% NDS	5% NDS
	anti-IL-36γ	Mouse	1:1600	Abcam, Cambridge, UK	Tris 110℃ 15min	Mouse stain Kit	5% NDS
	anti-IL-36Ra	Rat	1:200	R and D system, Minneapolis, MN, USA	Pepsin 37℃ 5min	10% NGS	5% NDS
	anti-IL-38	Rat	1:1500	R and D system, Minneapolis, MN, USA	Pepsin 37℃ 5min	10% NGS	5% NDS
Secondary antibody	Rat IgG-biotin	Goat	1:400	Biolegend, San Diego, CA, USA			
	Rabbit IgG-biotin	Goat	Undiluted	SABPO(R)Kit, Nichirei, Tokyo, Japan			
	Goat IgG-biotin	Donkey	1:200	Santa Cruz Biotechnology, Santa Cruz, CA, USA			
	Mouse IgG-biotin	Goat	Undiluted	Mouse stain Kit, Nichirei, Tokyo, Japan			
	Rabbit IgG-Alexa Fluor 488/546	Donkey	1:500	Thermo Fisher Scientific, Waltham, MA, USA			
	Rat IgG-Alexa Fluor 488/546	Donkey	1:500	Thermo Fisher Scientific, Waltham, MA, USA			
	Goat IgG-Alexa Fluor 488/546	Donkey	1:500	Thermo Fisher Scientific, Waltham, MA, USA			
	Mouse IgG-Alexa Fluor 488	Donkey	1:500	Thermo Fisher Scientific, Waltham, MA, USA			

Tris: 20mM Tris-HCl buffer (pH9.0). CB: 10mM citrate buffer (pH6.0). Pepsin: 0.1% pepsin. NDS: Normal donkey serum NGS: Normal goat serum α-SMA: Alpha-smooth muscle actin. IgG: Immunoglobulin G.

Supplemental table 2. Primers used in this study

Gene symbol (Accession)	Primer sequence (5'-3') F: Forward, R: Reverse	Product size (bp)
Actb (NM_007393)	F: TGTTACCAACTGGGACGACA R: GGGGTGTTGAAGGTCTCAAA	165
Il1f6 (NM_019450.3)	F: TCCTGCAGAACAATATCCTCAC R: GTTCGTCTCAAGAGTGTCCAGA	104
Il1f8 (NM_027163.4)	F: GTTCCTGCTAGCAACAATGTCA R: CCATCTCAACACAGCAGAAGC	142
Il1f9 (NM_153511.3)	F: CCAGTCAGCGTGACTATCCTC R: ATGGCTTCATTGGCTCAGG	193
Il1f5 (NM_001146087.1)	F: GAAGGATTCAGCCTTGAAGGTA R: CCGATTTGGGACAACACTG	112
Il1f10 (NM_153077)	F: TGGGAGACCCTGATTCAGACA R: TCTTTACACACGCCAGGCAG	132
Il1rl2 (NM_133193.3)	F: AGACACCTTAGAGTTCACCAGGAC R: CCATGGAAGAGTCACACCAG	163
Il1a (NM_010554.4)	AGATGACCTGCAGTCCATAACC GACAAACTTCTGCCTGACGAG	121
Il1b (NM_008361.4)	TTCCAGGATGAGGACATGAGC AATGGGAACGTCACACACCAG	111
Il1rn (NM_031167.5)	TTGTGCCAAGTCTGGAGATG TTCTCAGAGCGGATGAAGGTA	111
Il18 (NM_009360.2)	AGTAAGAGGACTGGCTGTGACC AACTCCATCTTGTTGTGTCCTG	174
Il33 (NM_001164724.2)	GCTGATGGTGAACATGAGTCC CTCCTATGTAAGTGCCAGGAAG	188

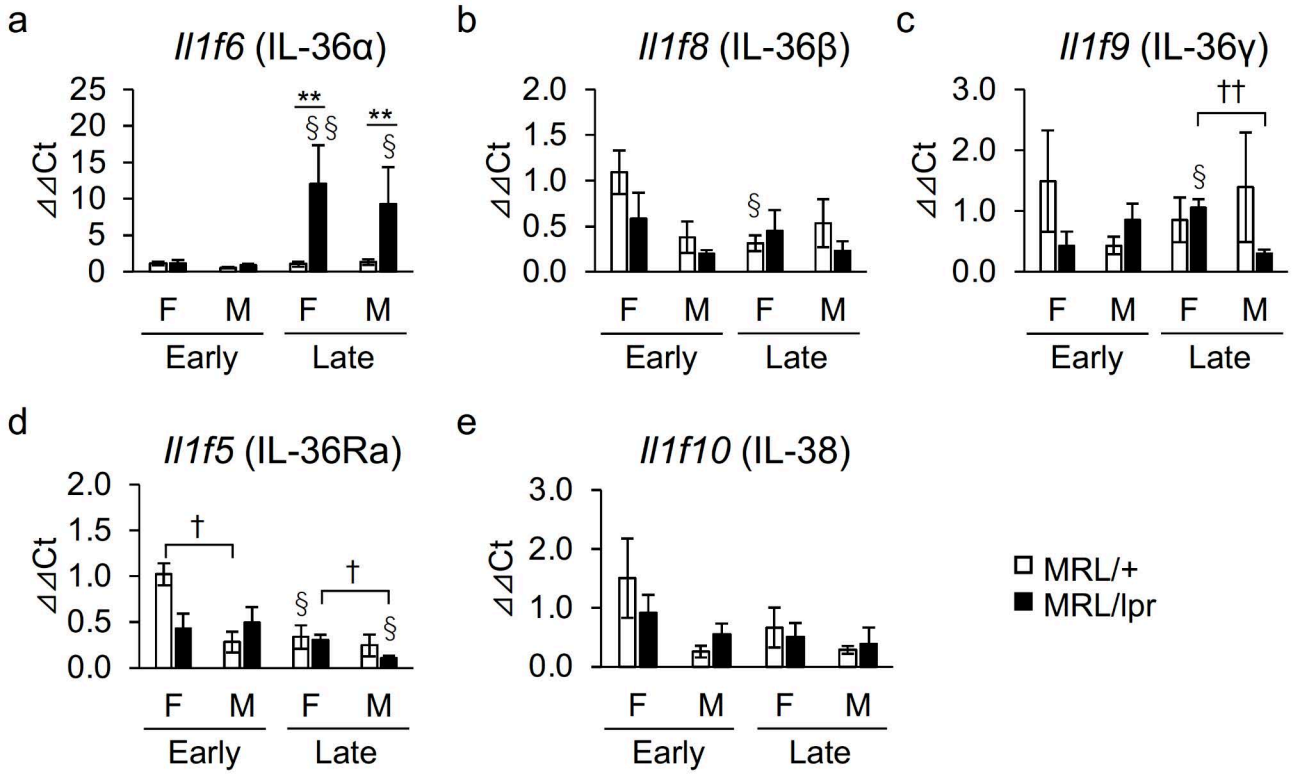
a
Il1f6 (IL-36α)
ΔΔCt
25
20
15
10
5
0
**
§§
**
§
F
M
F
M
Early
Late
b
Il1f8 (IL-36β)
ΔΔCt
2.0
1.5
1.0
0.5
0.0
§
F
M
F
M
Early
Late
c
Il1f9 (IL-36γ)
ΔΔCt
3.0
2.0
1.0
0.0
§
††
F
M
F
M
Early
Late
d
Il1f5 (IL-36Ra)
ΔΔCt
2.0
1.5
1.0
0.5
0.0
†
§
†
§
F
M
F
M
Early
Late
e
Il1f10 (IL-38)
ΔΔCt
3.0
2.0
1.0
0.0
F
M
F
M
Early
Late
MRL/+
MRL/lpr

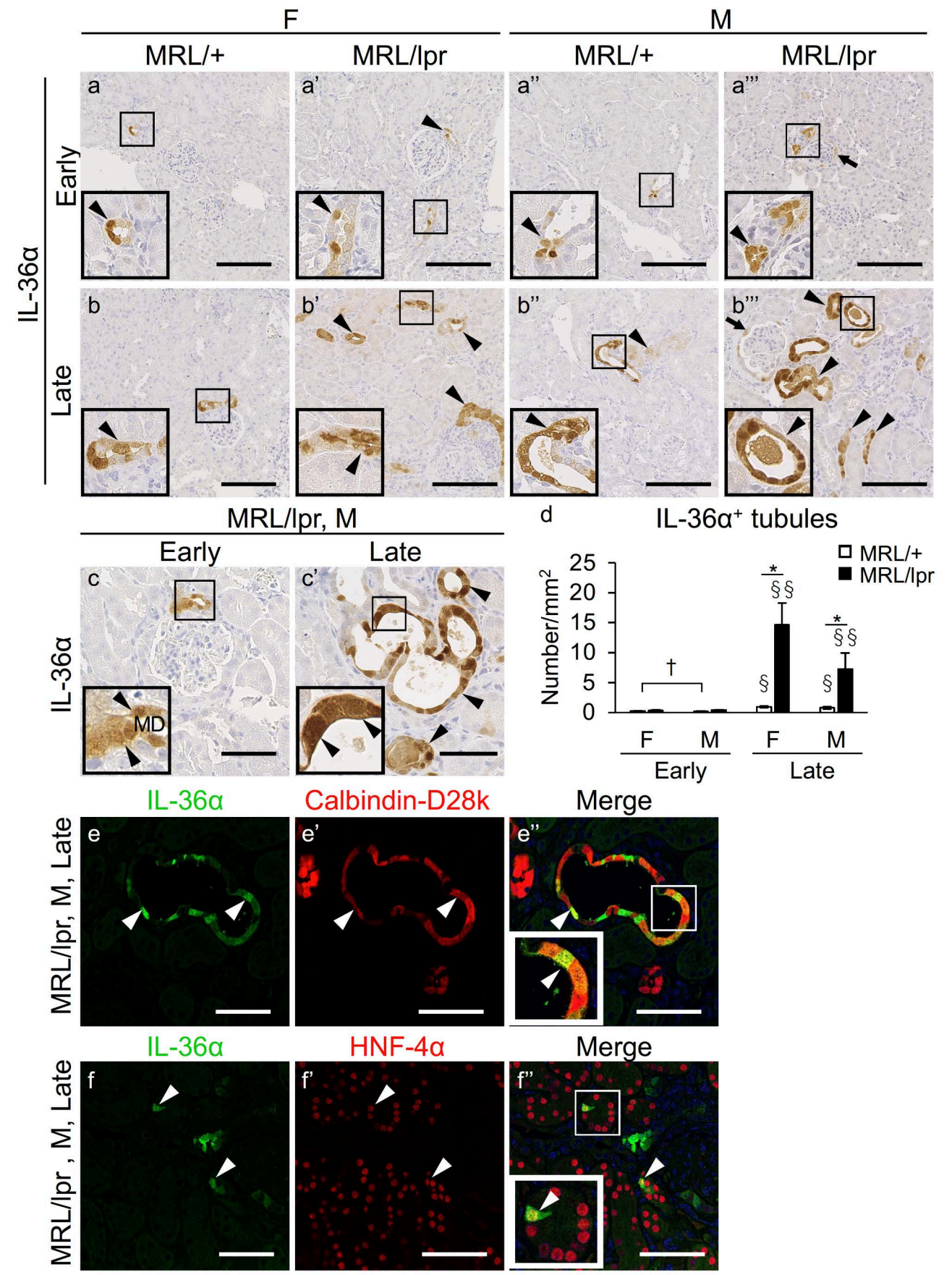
F
M
MRL/+
MRL/lpr
MRL/+
MRL/lpr
IL-36α
Early
Late
a
a'
a''
a'''
b
b'
b''
b'''
MRL/lpr, M
Early
Late
IL-36α
c
c'
MD
d
IL-36α⁺ tubules
MRL/+
MRL/lpr
Number/mm²
25
20
15
10
5
0
†
*
§§
§
F
M
F
M
Early
Late
IL-36α
Calbindin-D28k
Merge
MRL/lpr, M, Late
e
e'
e''
IL-36α
HNF-4α
Merge
MRL/lpr , M, Late
f
f'
f''

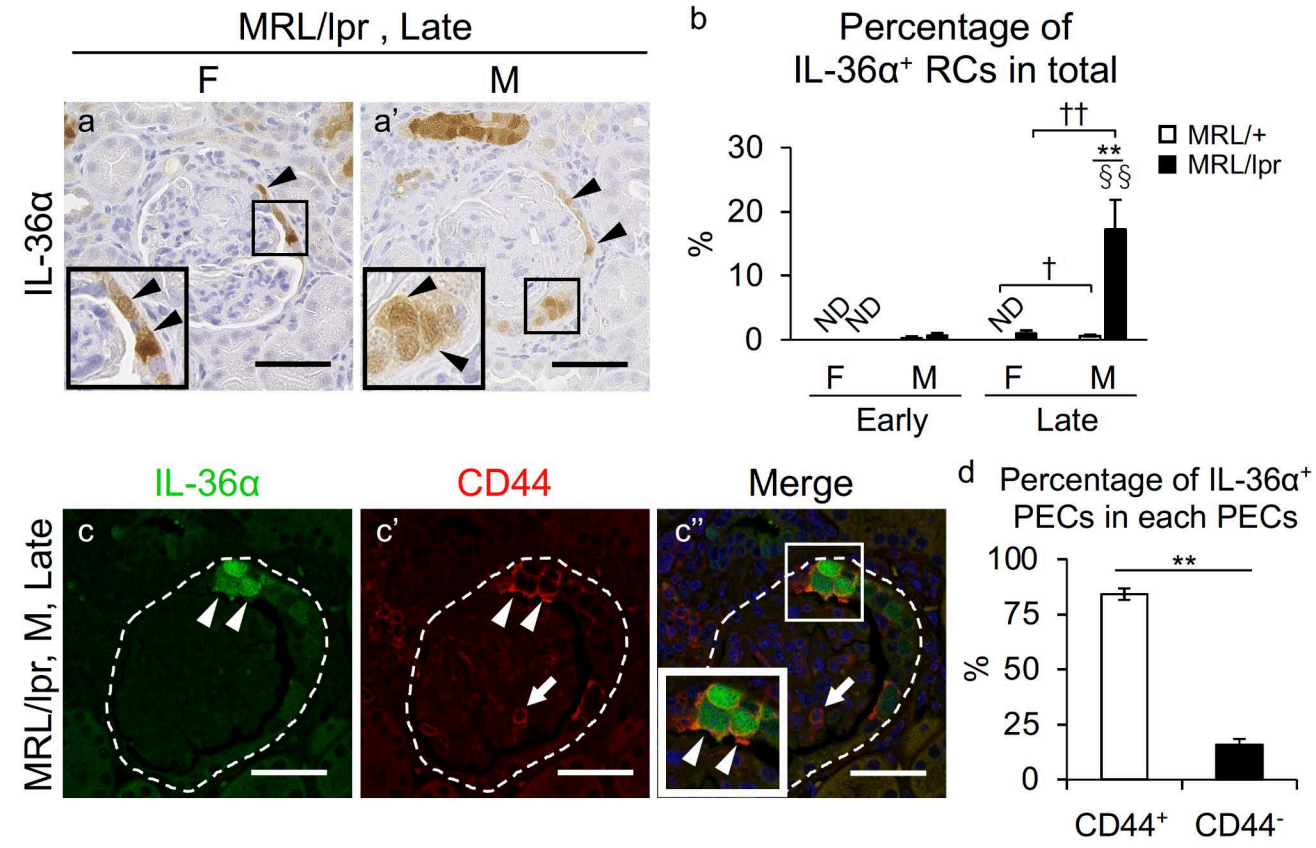
MRL/lpr , Late
F
M
IL-36α
a
a'
b
Percentage of
IL-36α⁺ RCs in total
MRL/+
MRL/lpr
%
30
20
10
0
ND
ND
ND
††
**
§§
†
F
M
F
M
Early
Late
IL-36α
CD44
Merge
MRL/lpr, M, Late
c
c'
c''
d
Percentage of IL-36α⁺
PECs in each PECs
100
75
50
25
0
%
**
CD44⁺
CD44⁻

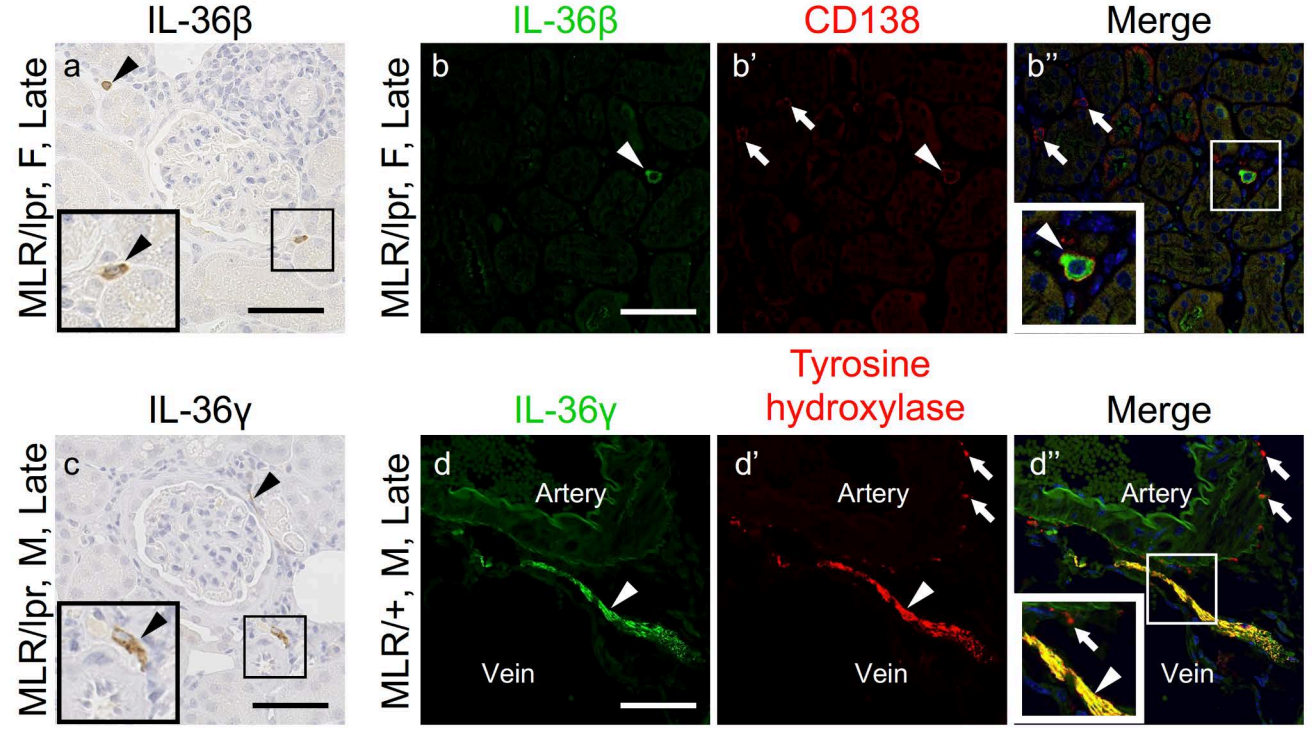
IL-36β
IL-36β
CD138
Merge
MLR/lpr, F, Late
a
b
b'
b''
IL-36γ
IL-36γ
Tyrosine hydroxylase
Merge
MLR/lpr, M, Late
MLR/+, M, Late
c
d
d'
d''
Artery
Vein

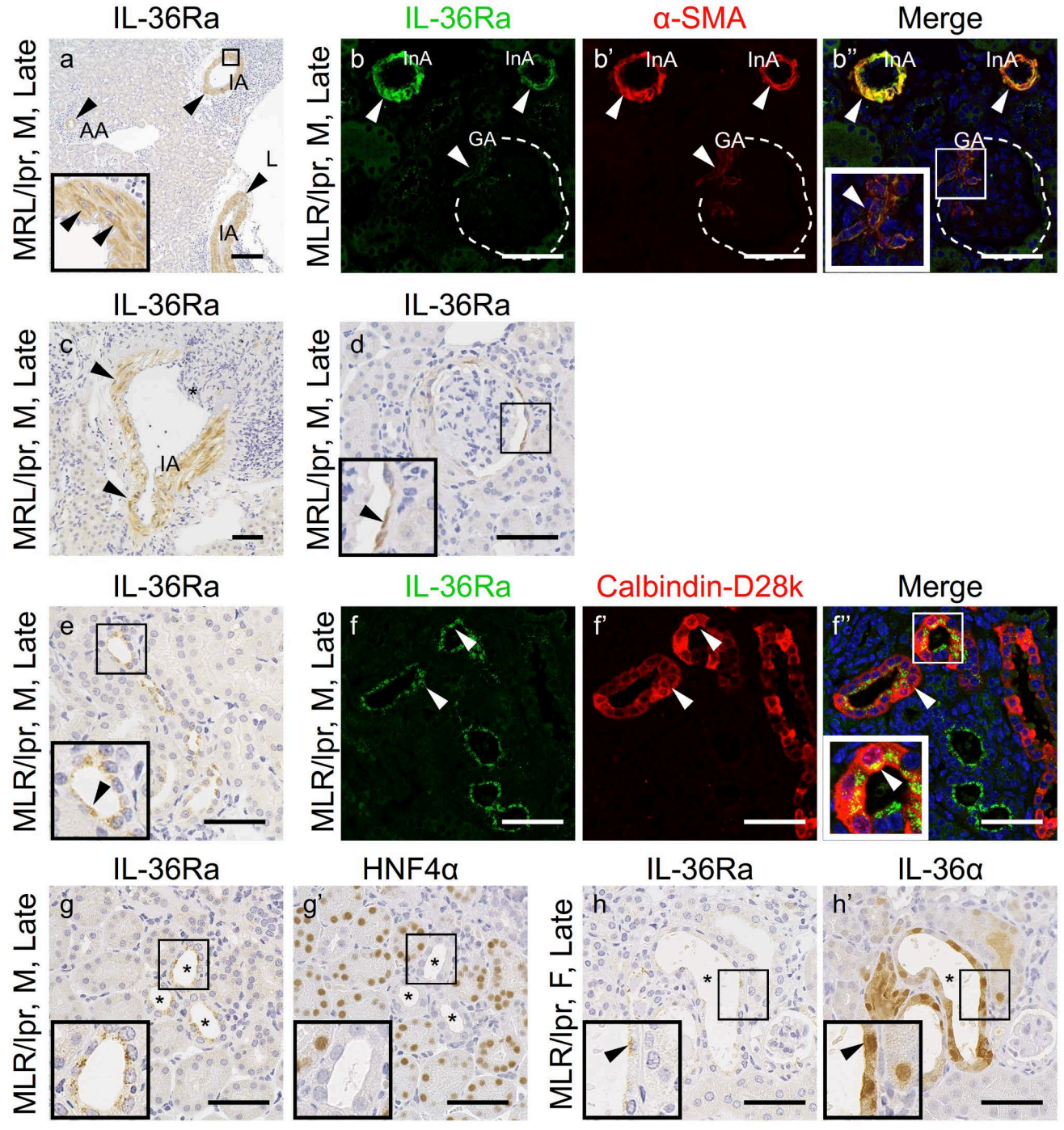
IL-36Ra
IL-36Ra
α-SMA
Merge
MRL/lpr, M, Late
a
AA
IA
L
IA
b
InA
InA
GA
b'
InA
InA
GA
b''
InA
InA
GA
MLR/lpr, M, Late
IL-36Ra
IL-36Ra
c
IA
d
MRL/lpr, M, Late
MRL/lpr, M, Late
IL-36Ra
IL-36Ra
Calbindin-D28k
Merge
e
f
f'
f''
MLR/lpr, M, Late
MLR/lpr, M, Late
IL-36Ra
HNF4α
IL-36Ra
IL-36α
g
g'
h
h'
MLR/lpr, M, Late
MLR/lpr, F, Late

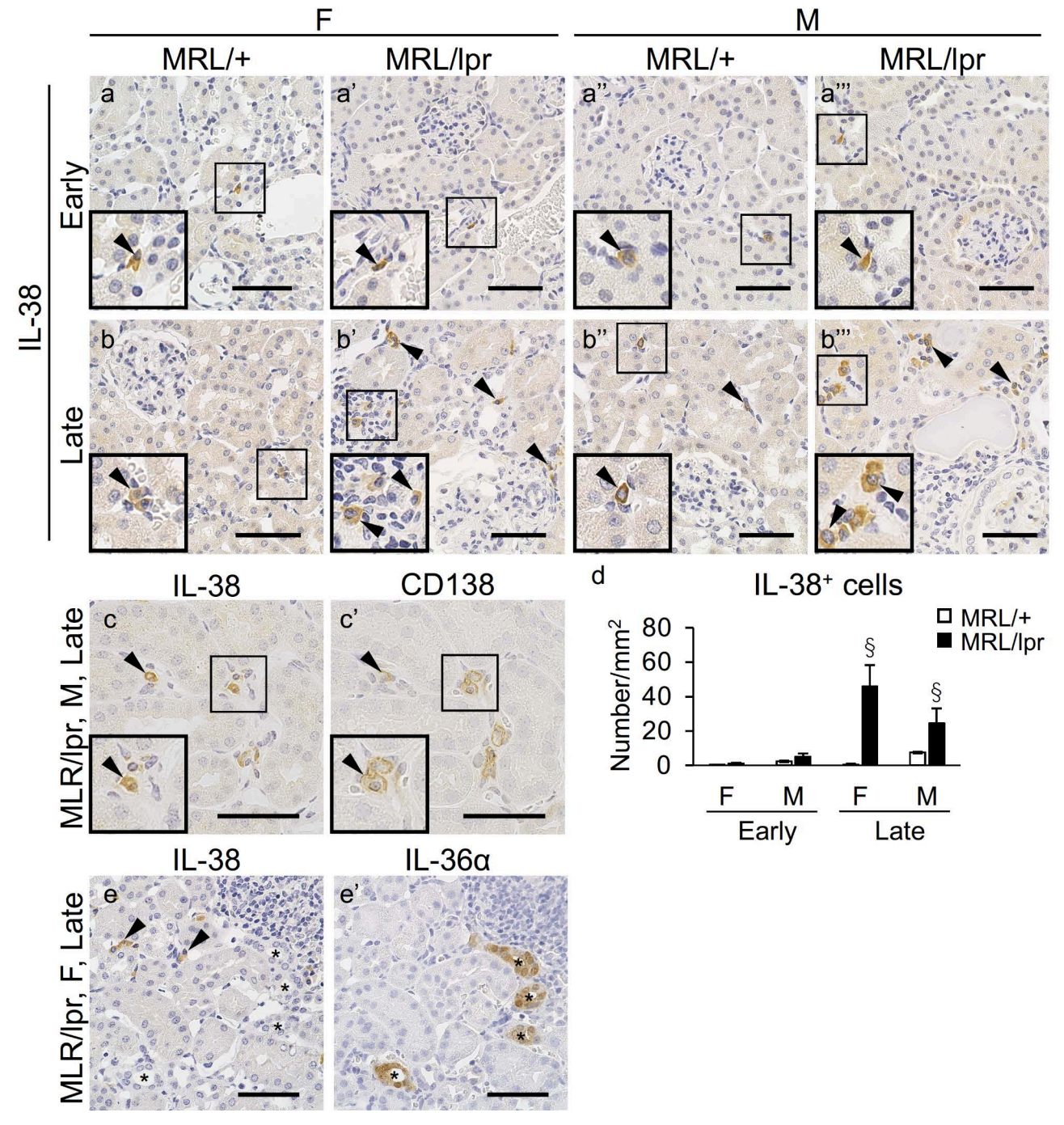
F
M
MRL/+
MRL/lpr
MRL/+
MRL/lpr
IL-38
Early
Late
a
a'
a''
a'''
b
b'
b''
b'''
IL-38
CD138
MLR/lpr, M, Late
c
c'
IL-38
IL-36α
MLR/lpr, F, Late
e
e'
d
IL-38+ cells
Number/mm2
80
60
40
20
0
MRL/+
MRL/lpr
§
§
F
M
F
M
Early
Late

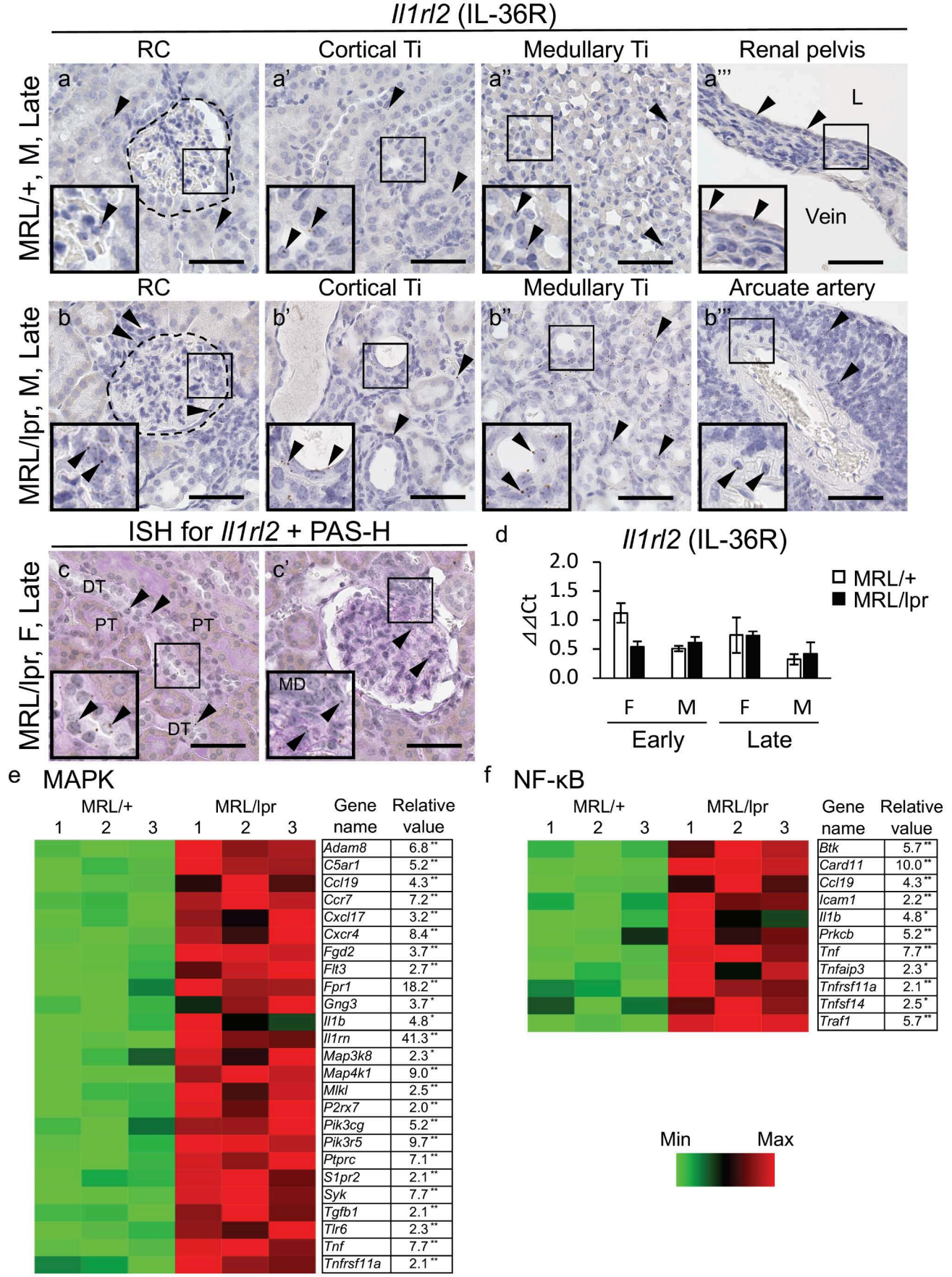
Il1rl2 (IL-36R)
RC
Cortical Ti
Medullary Ti
Renal pelvis
MRL/+, M, Late
a
a'
a''
a'''
L
Vein
RC
Cortical Ti
Medullary Ti
Arcuate artery
MRL/lpr, M, Late
b
b'
b''
b'''
ISH for Il1rl2 + PAS-H
MRL/lpr, F, Late
c
c'
DT
PT
PT
DT
MD
d
Il1rl2 (IL-36R)
ΔΔCt
2.0
1.5
1.0
0.5
0.0
MRL/+
MRL/lpr
F
M
F
M
Early
Late
e
MAPK
MRL/+
MRL/lpr
1 2 3 1 2 3
Gene name
Relative value
Adam8 6.8**
C5ar1 5.2**
Ccl19 4.3**
Ccr7 7.2**
Cxcl17 3.2**
Cxcr4 8.4**
Fgd2 3.7**
Flt3 2.7**
Fpr1 18.2**
Gng3 3.7*
Il1b 4.8*
Il1rn 41.3**
Map3k8 2.3*
Map4k1 9.0**
Mlkl 2.5**
P2rx7 2.0**
Pik3cg 5.2**
Pik3r5 9.7**
Ptprc 7.1**
S1pr2 2.1**
Syk 7.7**
Tgfb1 2.1**
Tlr6 2.3**
Tnf 7.7**
Tnfrsf11a 2.1**
f
NF-κB
MRL/+
MRL/lpr
1 2 3 1 2 3
Gene name
Relative value
Btk 5.7**
Card11 10.0**
Ccl19 4.3**
Icam1 2.2**
Il1b 4.8*
Prkcb 5.2**
Tnf 7.7**
Tnfaip3 2.3*
Tnfrsf11a 2.1**
Tnfsf14 2.5*
Traf1 5.7**
Min
Max

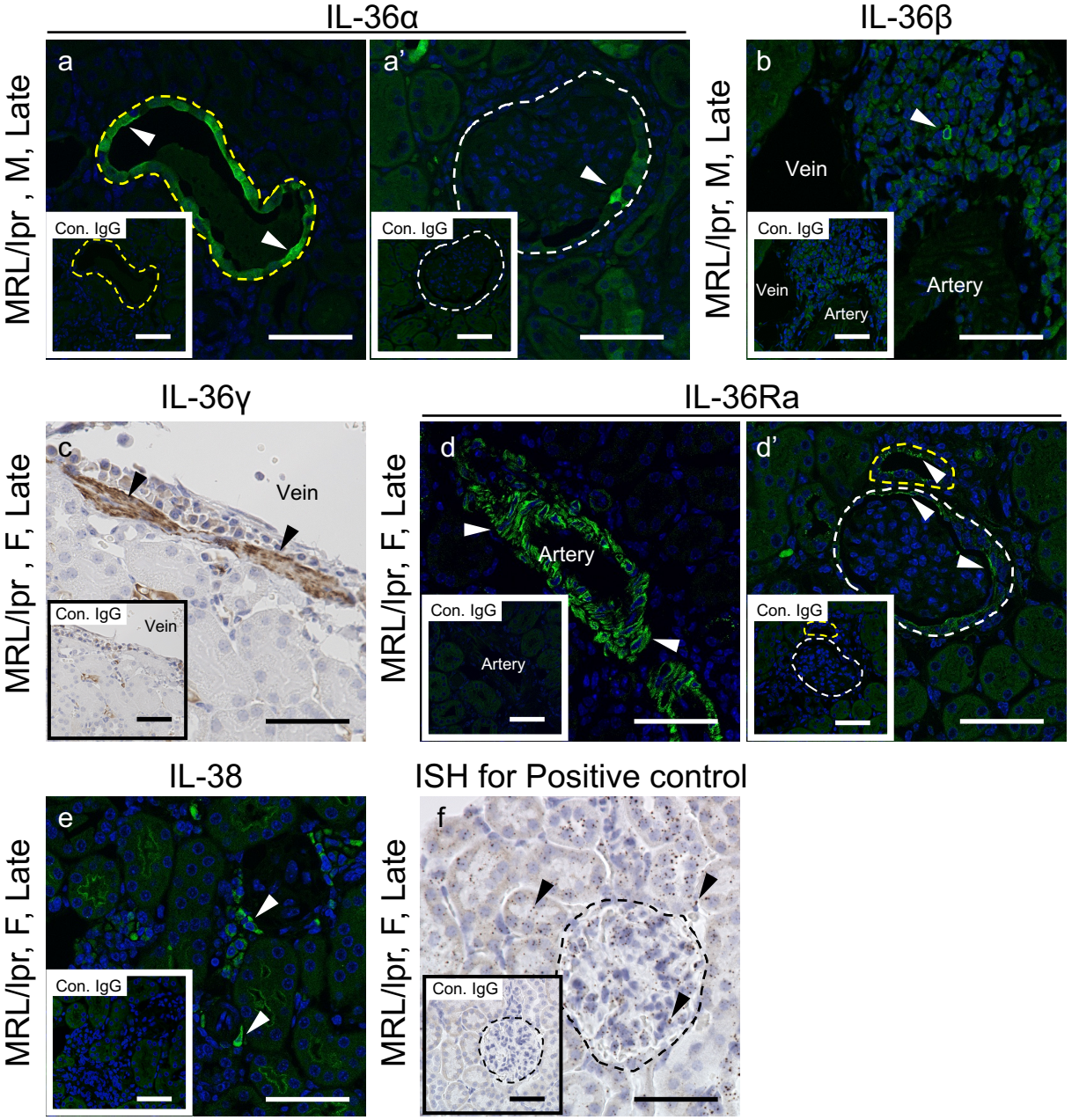

Supplemental Figure 1. Immunostaining for IL-36 subfamily members and *in situ* hybridization for positive control in the murine kidneys

(a-e) Representative immunostaining images for IL-36α, IL-36β, IL-36γ, IL-36Ra, and IL-38 in male and female MRL/lpr mice at the late stage of autoimmune nephritis. Insets indicate immunostaining using normal immunoglobulin G as a control corresponding to each primary antibody (Con. IgG). Arrowheads represent immuno-positive reactions. The yellow dotted line indicates the renal tubule. The white dotted line indicates the renal corpuscle. Bars= 50 mm. (f) Representative *in situ* hybridization (ISH) images for the positive control (*Polr2a*) in female MRL/lpr mice at the late stage. The inset indicates the images of the ISH image for the negative control (*DapB*). Bars= 50 μm. F: Female. M: Male. Late: Late stage autoimmune nephritis (6-7 months).

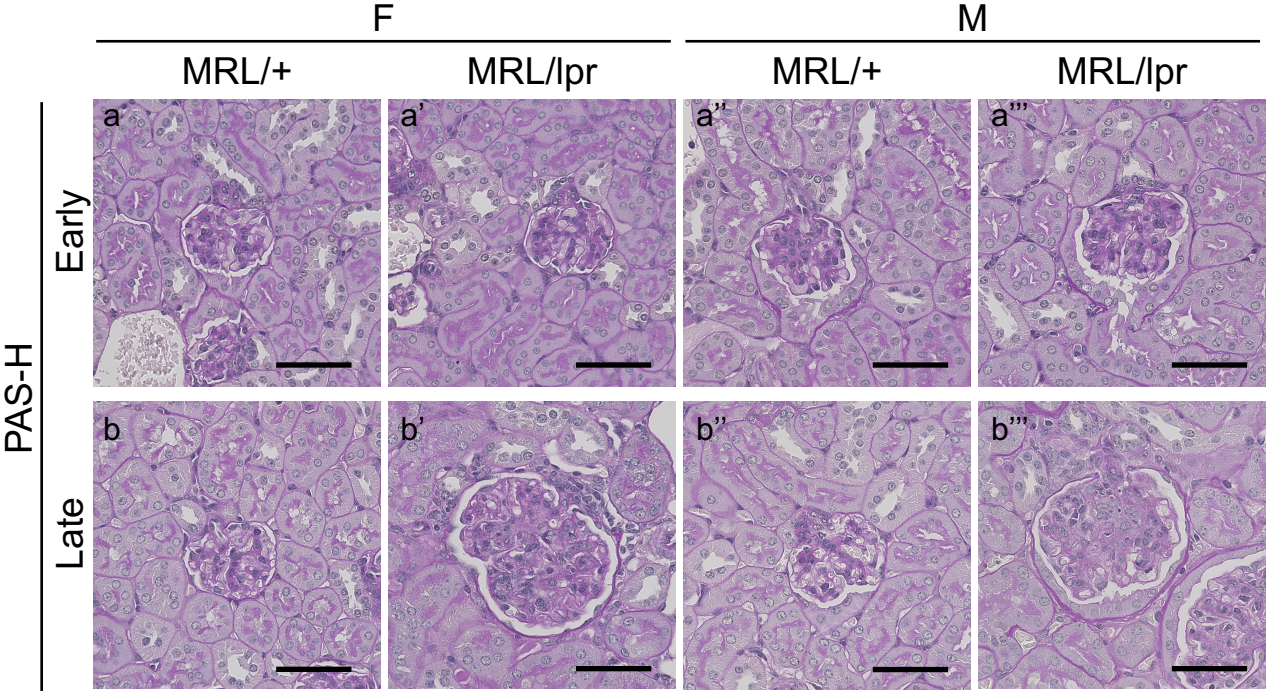

Supplemental Figure 2. Histopathology of glomeruli in the murine kidneys
(a-b’’’) Periodic acid Schiff hematoxylin (PAS-H) staining images for all groups. Glomerular hypercellularity and hypertrophy and mesangial matrix expansion are clearly observed in both sexes of MRL/lpr mice at the late stage of autoimmune nephritis. Bars= 50 μm. F: Female. M: Male. Early: Early stage of autoimmune nephritis (3 months). Late: Late stage autoimmune nephritis (6-7 months).

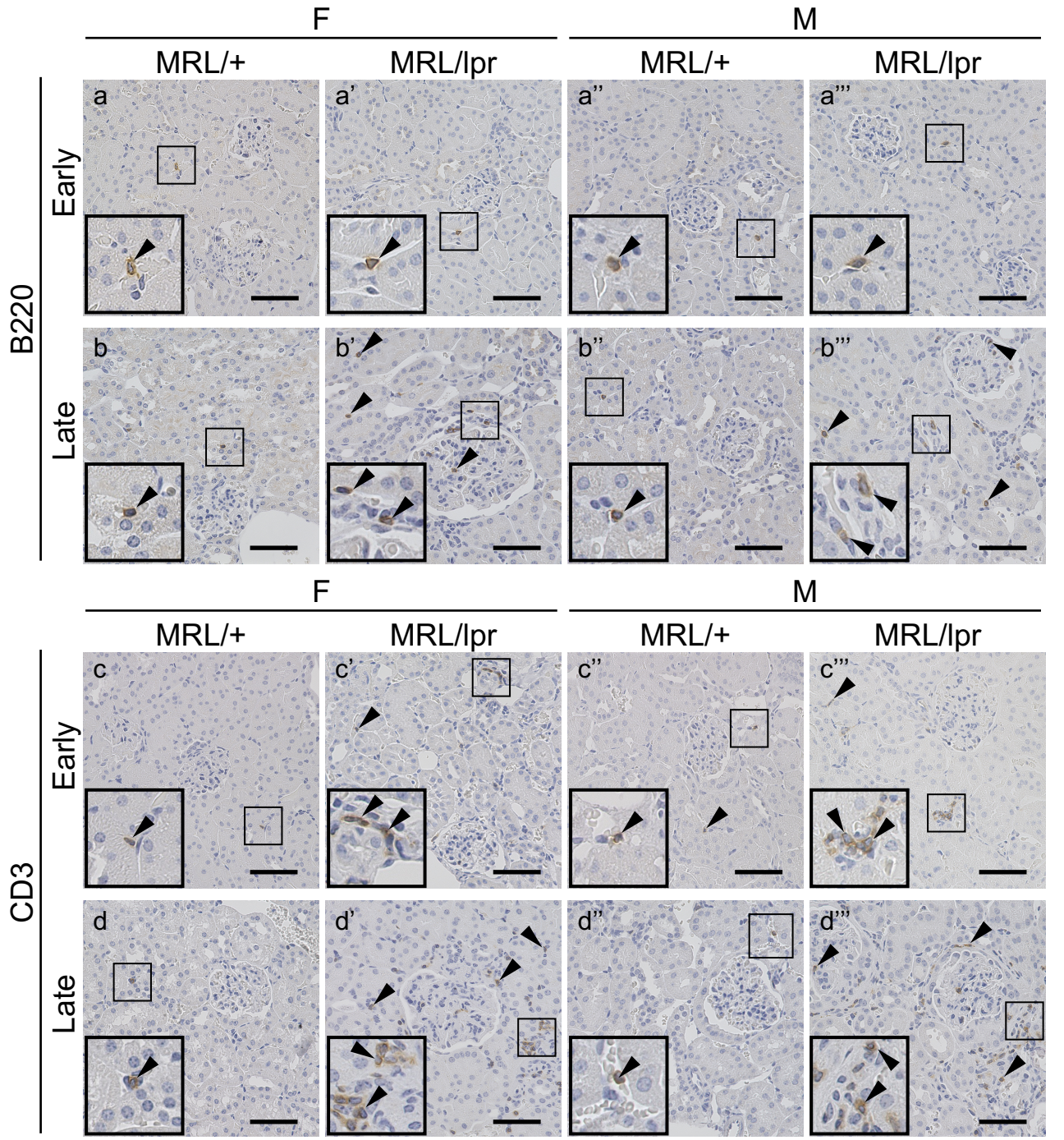

Supplemental Figure 3. Infiltration of B-cells and T-cells in the murine kidneys
(a-d''') Immunohistochemistry images for B220 (B-cell marker, panel a-b''') and CD3 (T-cell marker, panel c-d'''), respectively. Both $B220^+$ B cells and $CD3^+$ T-cells were abundant in the glomeruli and tubulointerstitium of both sexes of MRL/lpr mice at the late stage of autoimmune nephritis. Arrowheads indicate immune-positive cells. Insets indicate high magnification images of the areas marked by the black squares. Bars= 50 μm. F: Female. M: Male. Early: Early stage of autoimmune nephritis (3 months). Late: Late stage autoimmune nephritis (6-7 months).

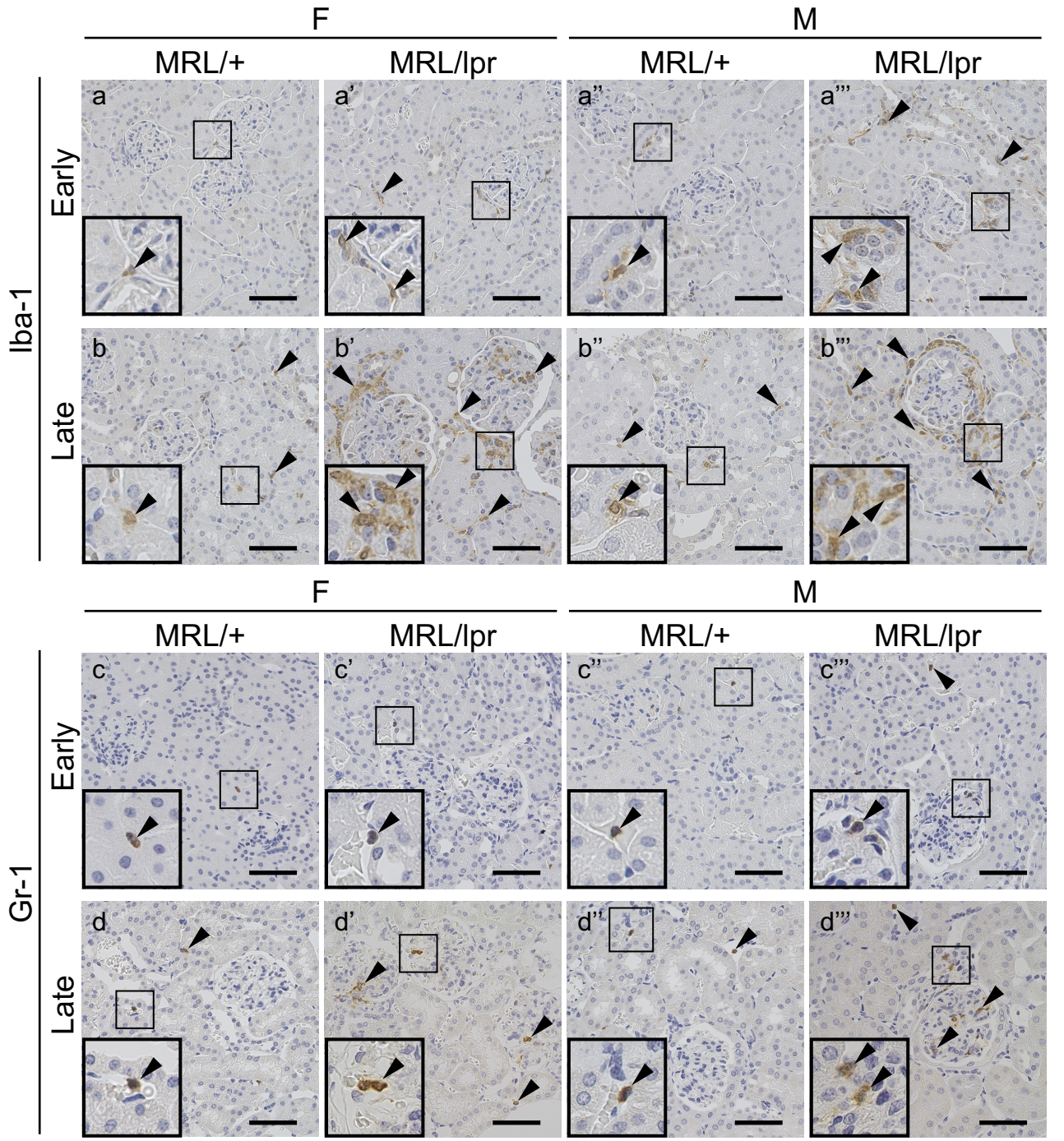

Supplemental Figure 4. Infiltration of macrophages and neutrophils in the murine kidneys (a-d''') Immunohistochemistry images for Iba-1 (macrophage marker, panel a-b''') and Gr-1 (neutrophil marker, panel c-d'''), respectively, for all groups. Iba-1^{+} macrophages and Gr-1^{+} neutrophils are abundant in the glomeruli and tubulointerstitium of both sexes of MRL/lpr mice at the late stage of autoimmune nephritis. Arrowheads indicate immune-positive cells. Insets indicate high magnification images of the areas marked by the black squares. Bars= 50 μm. F: Female. M: Male. Early: Early stage of autoimmune nephritis (3 months). Late: Late stage autoimmune nephritis (6-7 months).

	Early				Late			
	F		M		F		M	
	MRL/+	MRL/lpr	MRL/+	MRL/lpr	MRL/+	MRL/lpr	MRL/+	MRL/lpr
Il1a	1.431	0.742	0.923	0.728	0.840	0.760	0.591	0.677
Il1b	1.037†	1.554	0.619	0.922	0.932†	2.282*	0.511	1.098*
Il1rn	1.217	1.079	0.778	1.966	1.112	11.323** §	0.682	5.569*
Il18	1.124	1.414	1.178	0.870	0.905	1.758	1.203	1.382
Il33	1.099	0.948	0.550	0.782	1.139†	1.842	0.624	0.537

Supplemental Figure 5. mRNA expression of IL-1 family members in the murine kidneys
Relative mRNA expression levels of *Il1a*, *Il1b*, *Il1rn*, *Il18*, and *Il33* in the kidneys. The expression levels were normalized to the values of beta-actin (*Actb*) of female MRL/+ mice at the early stage of autoimmune nephritis. Each value represents the mean (n= 4-11). *: Significant difference in MRL/lpr mice against MRL/+ mice of the same sex at the same stage (*: $P < 0.05$, **: $P < 0.01$). † Significant difference in female versus male mice of the same strain at the same stage (†: $P < 0.05$). #: Significant difference at the late stage against the early stage in the same mouse strains of the same sex (#: $P < 0.05$). Mann-Whitney *U*-test. F: Female. M: Male. Early: Early stage of autoimmune nephritis (3 months). Late: Late stage autoimmune nephritis (6-7 months).

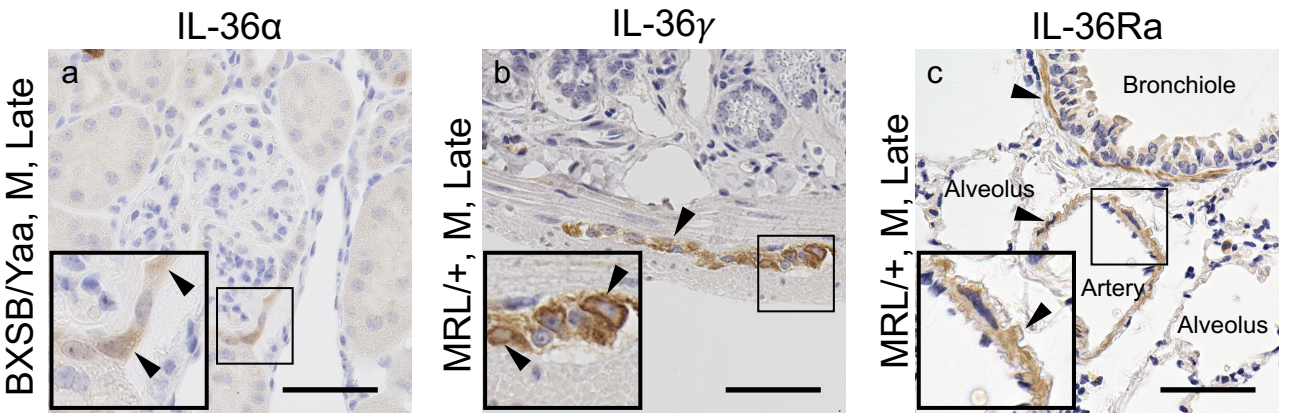

Supplemental Figure 6. Localization of IL-36α, IL-36γ, and IL-36Ra in other strains or other tissues
(a) Immunohistochemistry (IHC) image of IL-36α in the kidneys of male BXSB/MpJ-*Yaa* (BXSB/Yaa) mice at the late stage of autoimmune nephritis. The IL-36α$^+$ reaction (arrowhead) is observed in male BXSB/Yaa mice at the late stage of autoimmune nephritis. Bars= 50 μm. (b) IHC image of IL-36γ in the jejunum of male MRL/+ mice at the late stage. The IL-36γ$^+$ reactions (arrowheads) are observed in the myenteric nerve plexus. Bars= 50 μm. (c) IHC image of IL-36Ra in the lungs of male MRL/+ mice at the late stage. The IL-36Ra$^+$ reactions (arrowheads) are observed in the smooth muscle layers of arteries and bronchioles. Insets indicate high magnification images of the areas marked by the black squares. Insets indicate high magnification images of the areas marked by the black squares. Bars= 50 μm. M: Male. Late: Late stage of autoimmune nephritis (6-7 months).

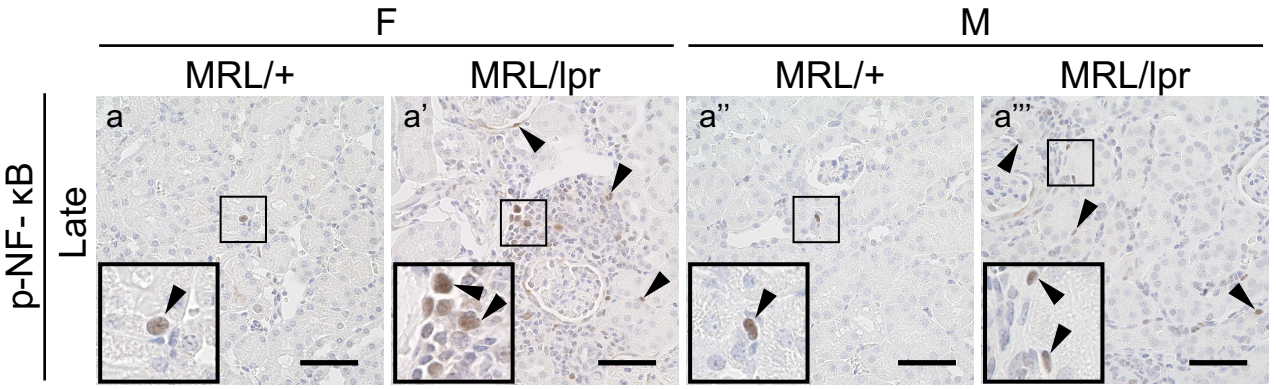

Supplemental Figure 7. Localization of phosphorylated nuclear factor kappa B (p-NF-κB) in the murine kidneys

(a-a''') Representative immunohistochemistry (IHC) images for p-NF-κB. p-NF-κB^{+} nuclei (arrowheads) are observed in renal tubular and parietal epithelial cells, and infiltrated cells of all groups at the late stage of autoimmune nephritis, and that number is abundant in both sexes of MRL/lpr mice compared to MRL/+. Insets indicate high magnification images of the areas marked by the black squares. Bars= 50 μm. F: Female. M: Male. Late: Late stage of autoimmune nephritis (6-7 months).